CERN-ACC-NOTE-2020-0059
xavier.buffat@cern.ch

Strategy for Landau damping of head-tail instabilities at top energy in the HL-LHC

X. Buffat, S. Antipov, G. Arduini, R. De Maria, N. Karastathis, S. Kostoglou, A. Koval, E. Maclean, E. Métral, N. Mounet, Y. Papaphilippou, T. Persson, R. Tomás, CERN, Geneva, Switzerland

Abstract

The main aspects linked to Landau damping of head-tail instabilities at top energy in the HL-LHC are discussed, in particular the interplay between the arc octupoles and long-range, offset or head-on beam-beam interactions as well as lattice imperfections. When possible, the models are compared with the operational experience of Runs 1 and 2 of the LHC. Based on these considerations, various operational scenarios are discussed identifying their strengths and limitations.

Geneva, Switzerland
November 24, 2020

Contents

1 Introduction

The HL-LHC project [1], the high luminosity upgrade of the LHC, poses a number of challenges linked to the stability of the beams in the transverse plane, mainly due to the increase in beam intensity. The current operational scenario [2] relies on the combination of the transverse damper, a high chromaticity and Landau damping in order to stabilise head-tail instabilities driven by the machine impedance, similarly to the current LHC. Numerous aspects linked to Landau damping revealed their importance during the first two runs of the LHC. This note addresses their impact on the operation of the HL-LHC.

Currently the stability threshold of the LHC and HL-LHC beams at top energy is estimated based on the comparison of the estimation of the complex coherent tune shifts induced by the wake fields and the estimation of the strength of Landau damping induced by the spread in the tune of the individual particles due to the various non-linear fields that they experience. Both derivations are based on the introduction of a perturbation with respect to the linear model, respectively either the wake fields or the tune spread. The first provides a set of complex tune shifts for the different coherent modes of oscillation with respect to their unperturbed frequencies, usually obtained by solving numerically the Vlasov equation written as an eigenvalue problem [3]. In the approximation that the modes of oscillation remain close to the unperturbed ones and that the coupling between them can be neglected, the complex tune shift in the presence of a tune spread can be written as a function of the unperturbed coherent tune shift (i.e. perturbed by the wake fields, but not by the tune spread) via the dispersion relation [4], written without loss of generality for the horizontal plane:

$$-\frac{1}{\Delta Q_{c,x}} = \int \frac{J_x \frac{\mathrm{d}\Psi(J_x,J_y)}{\mathrm{d}J_x}\mathrm{d}J_x\mathrm{d}J_y}{\Delta Q_{LD,x} - \Delta Q_{i,x}(J_x,J_y)} \tag{1.1}$$

where $\Delta Q_{c,x}$ and $\Delta Q_{LD,x}$ are the horizontal unperturbed coherent tune shift and the corresponding complex tune shift including the effect of Landau damping respectively. The transverse actions J_x and J_y were introduced along with their distribution function $\Psi(J_x,J_y)$ and the transverse detuning with amplitude $\Delta Q_{i,x}(J_x,J_y)$ of individual particles. We note that, since we are considering high energy beams, the contribution of space-charge forces is neglected. The second order chromaticity is also neglected in this formalism. This assumption is conservative since the second order chromaticity mostly introduces additional damping [5, 6].

The strength of Landau damping is conveniently represented independently of the unperturbed coherent tune shifts using the area in the complex plane defined by

$$\{\Delta Q \in \mathbb{C} : \Re\Delta Q = \Re\Delta Q_{c,x}(\Delta Q_{LD,x}) \;\Rightarrow\; \Im\Delta Q \leq \Im\Delta Q_{c,x}(\Delta Q_{LD,x}) \;\forall\, \Delta Q_{LD,x} \in \mathbb{R}\}. \tag{1.2}$$

This area represents the unperturbed complex tune shifts ΔQ that can be stabilised by Landau damping and thus is often called the stability diagram. We note that the integral has to be evaluated with a positive infinitesimal imaginary part added to the denominator [7, 8] (by convention positive imaginary tunes corresponds to modes with exponentially growing amplitudes).
The stability limits are often quoted in terms of octupole current. However in the presence of other non-linear forces, such as beam-beam interactions, the stability diagram may become a rather intricate function of several parameters. In order to conveniently compare the stability limit in different configurations, we shall characterise each configuration with the coherent stability factor [9]. The stability factor $\mathcal{I}$ is the ratio of the modulus of the actual tune shift to the modulus of maximum tune shift with the same argument that can be stabilised by Landau damping. In other words, for a stable configuration the stability factor is below 1 and the impedance could be multiplied by a factor up to $1/\mathcal{I}$ without getting any instability.

Within this theory, three elements are key in the establishment of the stability threshold:

- The coherent tune shift due to the wake fields, mainly determined by the bunch intensity, the longitudinal dynamics, the chromaticity, the beam coupling impedance of all the elements composing the machine, summed into a so-called impedance model, as well as the transverse damper.
- The beam distribution function, usually but not exclusively assumed to be Gaussian in physical space, i.e. exponential in action, is mainly represented by the r.m.s. transverse emittances.
- The amplitude detuning, dependent on all the non-linear elements in the machine, in particular the arc octupoles meant for that purpose (also called Landau octupoles) [10], but also unwanted contributions such as those of beam-beam interactions and magnet field errors.

This note focuses on the aspects related to the amplitude detuning as the impedance models for the LHC and HL-LHC are detailed in [11–13]. Also, Gaussian distributions with over or under populated tails will be considered in the following, as more involved modifications of the beam distribution, in particular under the influence of external sources of noise, are the subject of recent developments [14, 15]. The impact of the latter on the strategy for Landau damping will be evaluated based on the new models once fully established.
We note also that, as coherent aspects of beam-beam interactions were already addressed in [9], in the following only the incoherent aspects of beam-beam interactions, i.e. their impact on the amplitude detuning, will be discussed.

The observations of instabilities at top energy over the first two runs of the LHC are reviewed in the next section with an emphasis on the main differences observed when operating with the two polarities of the octupoles. The strategies for Landau damping over the HL-LHC cycle are discussed in light of these observations and their understanding.
By convention the polarity of the octupoles refers to the sign of the current in the focusing magnets (LOF). Thus, the negative or positive polarity generates a negative or positive direct detuning with amplitude respectively.

2 Models and observations at LHC

2.1 Non-colliding beams

2.1.1 Impact of the transverse tails

The impact of the tail of the beam distribution on the stability diagram generated by the arc octupoles is discussed in [16]. It was found that, in the case of Gaussian beams, the negative polarity is favourable for the stabilisation of coherent modes with negative real tune shifts, as expected for LHC and HL-LHC [11, 13]. This difference is increased in the presence of a large population in the tail, favourable only with the negative polarity. On the other hand, since halo depletion techniques are considered for the HL-LHC [1], the stability threshold estimates will consider a Gaussian beam distribution cut at 3 σ. This assumption is rather pessimistic as it is planned to actively deplete the distribution only above 4.7σ (for a normalised emittance of 2.5 μm) [17]. Additionally a full depletion is likely not achievable. Nevertheless, it is justified by the large unknowns on the resulting beam distribution. As shown in Fig. 1, the cutting of the tails leads to instability thresholds at approximately 25% higher current when operating with the positive polarity. With the negative polarity, the ratio of the instability thresholds with and without tails can reach approximately 2.5.

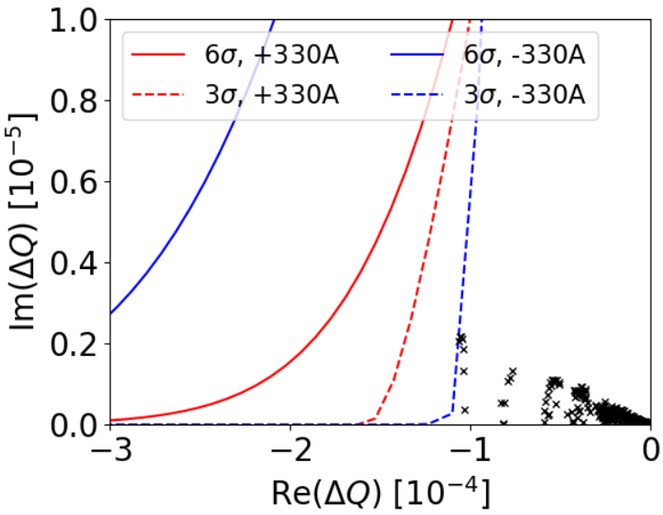

Figure 1: Stability diagrams for a non-telescopic optics at flat top and considering Gaussian transverse distributions cut at 3 and 6 σ. The complex tune shift of the modes that require stabilisation by Landau damping are marked with black crosses for illustration. The machine and beam parameters are those of the ultimate scenario with BCMS beams [9] with the baseline impedance model including the collimator upgrade and the crab cavities [12].

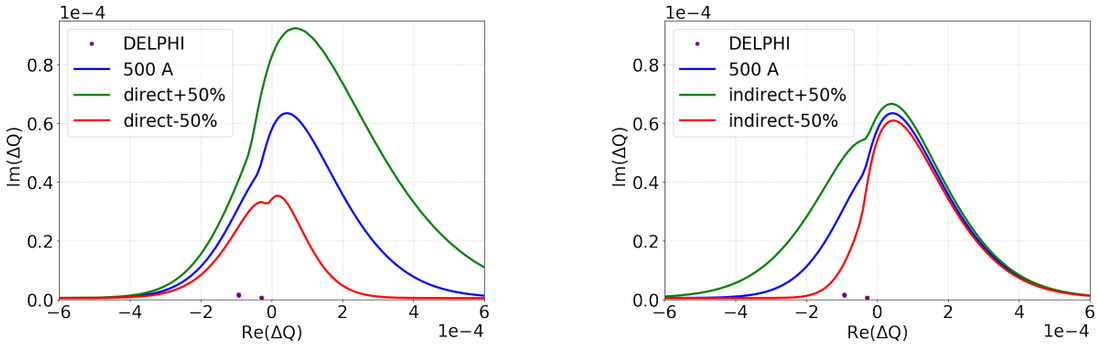

Figure 2: Stability diagrams with +500 A in the octupoles for transverse emittances of 1 μm (blue), compared to the same configuration with the direct or indirect terms (left and right plots) amplified by a factor 0.5 and 1.5 (red and green curves). Reversing the polarity of the octupole would lead to the stability diagram obtained by the mirror symmetry with respect to the vertical y-axis. Purple dots represent the complex tune shifts of the most unstable modes. They were obtained with DELPHI based on the baseline HL-LHC impedance model (Sec. 3.1) for chromaticities between 10 and 15 units.

2.1.2 Non-linear optics correction

At top energy, the effect of most magnet's non-linearities is significantly suppressed with respect to injection energy mostly by the adiabatic damping of the transverse emittance. On the other hand, the errors in the magnets of the low β insertions and in particular the final focusing triplets are enhanced by the betatron squeeze. Their impact on the amplitude detuning can become comparable to the one of the arc octupoles, both directly or indirectly, e.g. through feed-down effect to linear coupling [18]. These effects are the strongest at the lowest β^* thus favouring the establishment of collision at a high β^* for luminosity levelling. Indeed, once in collision the tune spread generated by head-on interactions is sufficiently large to overcome the effect of the lattice non-linearities. This is however not the case for bunches that are non-colliding even on collisional orbits, i.e. bunches lacking colliding partners in the other beam. These bunches are needed for background measurements in the different detectors [19]. Their brightness is not significantly affected during luminosity production due to lack of luminosity burn off. Therefore, as opposed to colliding bunches, their need for Landau damping remains constant until the end of the cycle. Instabilities of the non-colliding bunches observed in 2018 during the last β^* levelling step to 25 cm when operating with a reduced tune separation for lifetime optimisation [20] can be attributed to the impact of the triplet non-lineraities.

When an ideal correction can not be achieved, the correction of the direct or indirect terms should be favoured when operating the octupoles with the negative or positive polarity respectively. This effect is

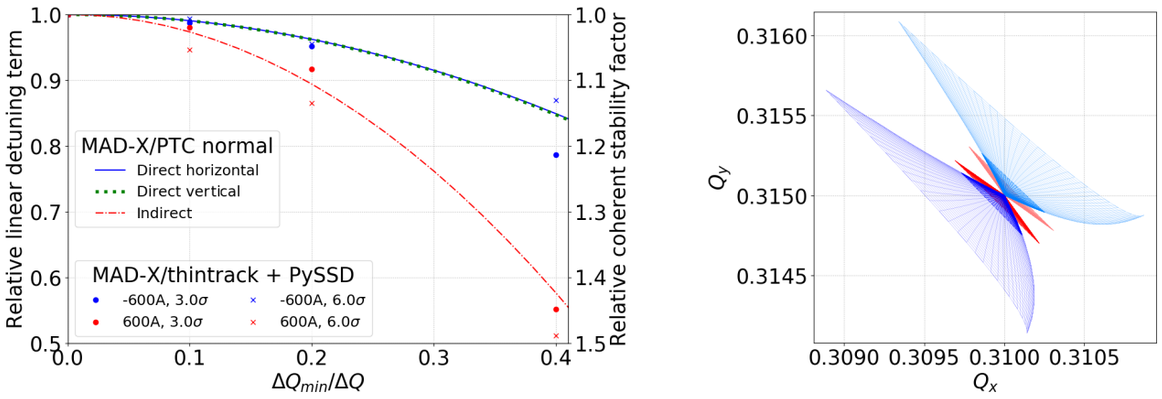

(a) (b)

Figure 3: Relative variation of the linear amplitude detuning terms obtained with MAD-X/PTC normal [21, 22] using the 2018 LHC optics [23] introducing linear coupling with the arc sextupoles (lines on the left plot). The global coupling knobs were used, choosing the phase having the largest impact on amplitude detuning. The variation of the stability factor obtained with MAD-X/thintrack and PySSD using the same optics and the coherent tune shifts corresponding to the HL-LHC impedance model are shown with dots and crosses on the left plot, corresponding to two different cuts in the Gaussian distribution used to compute the stability diagram. The corresponding tune footprints for $\Delta Q = 0.005$ and $\Delta Q_{min}/\Delta Q = 0$ or 0.4 are shown on the right plot with red and blue curves respectively. The footprints expanding to the upper right with lighter colors correspond to an octupole current of 600 A, the ones pointing to the lower left to -600 A. The solid parts of the footprints correspond to particles oscillating with amplitudes between 0 and 3 σ. The shaded parts of the blue footprints correspond to particles oscillating with amplitudes between 3 and 6 σ.

illustrated in Fig. 2, which can be understood intuitively as the negative detuning term (direct and indirect for the negative and positive polarity respectively) dominates the stability diagram in the negative real tune shifts.

2.1.3 Coupling

Independently of the polarity of the arc octupoles, an important reduction of the stability diagram is expected in the presence of linear coupling when operating with close fractional tunes in the two transverse planes [24]. On the other hand, close tunes are usually favourable for the beam lifetime once in collision [25]. Therefore, the optimal scheme relies on the proper balance between these constraints. Figure 3a shows the worst relative reduction of the linear amplitude detuning terms due to linear coupling in the regime of small coupling, i.e. the difference between the transverse tunes ΔQ is much larger than the closest tune approach driven by linear coupling ΔQ_{min}. In this regime, the Landau damping is dominated by the linear contribution of coupling, as confirmed by the comparison with estimates of Landau damping based on single particle tracking simulations which include higher order effects. In particular, the Amplitude Dependent Closest Tune Approach (ADECTA) [26] affects mainly particles at large amplitude in this regime, such that they do not impact Landau damping significantly. Yet, other components leading to ADECTA such as skew octupolar terms [26] can have a detrimental impact on the stability diagram [27], thus their correction to a level that they do not affect low amplitude particles, i.e. below 3σ, is required.

2.1.4 Operational experience

In 2012, the effect of the non-linearities in the Interaction Region (IR) remained uncorrected during operation. Accurate measurements of the amplitude detuning were performed in various conditions during Run 2 using the AC-dipole method [18]. Since this method was in development in Run 1, the measurement are scarce. In particular, no measurements are available with a crossing angle in Run 1. Thus, the extrapolation of Run 2 measurements with crossing angles to the operational configuration of Run 1 suffers from significant uncertainties even assuming that the errors have remained identical. Indeed, the exact nature of the source of the amplitude detuning measured in Run 2 is not known, affecting the scaling with β^* and with the crossing angle, especially since the latter changed polarity in IP1 between the runs. Nevertheless, based on the most pessimistic considerations the amplitude detuning may have reached an equivalent of 80 A in the arc octupoles, representing at most 15% of the current used operationally in 2012. This contribution is therefore not sufficient to explain the stability issues observed in 2012.

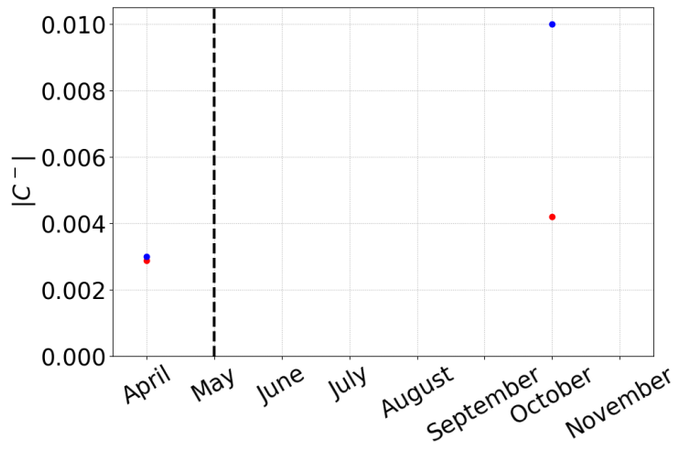

Figure 4: Measurements of linear coupling performed with the AC dipole in 2012 (blue and red dots for B1 and B2 respectively). The vertical dashed line shows the time of the only trim of the skew quadrupoles done over the year (details in [28]).

On the other hand, linear coupling was accurately measured with the AC-dipole and corrected globally only once during the commissioning. It was measured a second time at the end of the year, these measurements are reported in Fig. 4. The drifts were therefore uncontrolled through the year. The strong variation from the start to the end of the year may be attributed first to an inaccurate correction applied right after the technical stop 1 in both beams, potentially increasing the linear coupling above $\Delta Q_{min} = 6 \cdot 10^{-3}$ and $\Delta Q_{min} = 2 \cdot 10^{-3}$ in B1 and B2 respectively. The strength of this trim is however not sufficient to explain the linear coupling around 10^{-2} measured at the end of the year in B1. The contributions of the triplets to linear coupling at the end of the squeeze were estimated based on hourly measurements of their tilt angles, yielding a slow evolution by approximatively $3 \cdot 10^{-3}$ over the year [28]. These contributions might add or subtract to the other sources of linear coupling depending on their relative phase advances, which are not known. Nevertheless, the scarce measurements are compatible with an unfavourable drift in B1, leading to the large linear coupling measured at the end of the year and a favourable drift in B2. In such conditions, it is expected that the required octupole current for B1 is increased by large factors at the end of the squeeze when operating with a tune separation in the order of 10^{-2}.
The gated transverse damper and BBQ were introduced for standard operation in Run 2 to overcome a strong limitation on the tune accuracy when operating with high intensity beams observed in Run 1 [29, 30] which potentially led to tune separations between $0.6 \cdot 10^{-2}$ to $1.4 \cdot 10^{-2}$ when operating with collision tunes, i.e. during the squeeze, collapse of the separation bumps and collision. The combination of large linear coupling and lack of control of the tune separation results in a lack of control on Landau damping, potentially leading to strong fill to fill variations.

The loss of Landau damping by linear coupling is likely the main cause of most of the instabilities observed in 2012, both at the end of the squeeze and during ADJUST. The latter will be discussed in the next chapter. We shall note that some instabilities were observed at top energy in 2012 before the change from the injection working point, featuring a large tune separation (≈ 0.03), to the collision working point featuring a reduced tune separation (≈ 0.01) and before the betatron squeeze. In these conditions, the effects of linear coupling, lattice non-linearities or even beam-beam interaction are not expected to affect significantly Landau damping. These instabilities were observed with either polarity of the octupoles, but seemed to have disappeared when operating with chromaticities higher than 10 units [31]. In Run 2, the octupoles current at the stability threshold of single bunches has been measured significantly higher than expected with chromaticities close to 0 [32]. Presently the mechanism leading to this high octupole strength requirement with low chromaticities is not understood. The modifications of the longitudinal distribution resulting from the active longitudinal blow up in the ramp, in particular their impact on the transverse stability threshold, was suspected following studies conducted for the HL - LHC [33]. The strength of this effect seems however too weak to be compatible with the obervations at the LHC [34]. Consequently, the chromaticity of 15 units used in the second part of 2012 and through Run 2 is maintained as the baseline for non-colliding beams based on empirical observations only. In this regime, the experimental data obtained through Run 2 are compatible with the predictions of the instability model within a factor 2 [35]. This empirical factor is accounted for in the HL-LHC design. Practically speaking, it means that we aim at a design featuring a stabilty factor below 0.5.

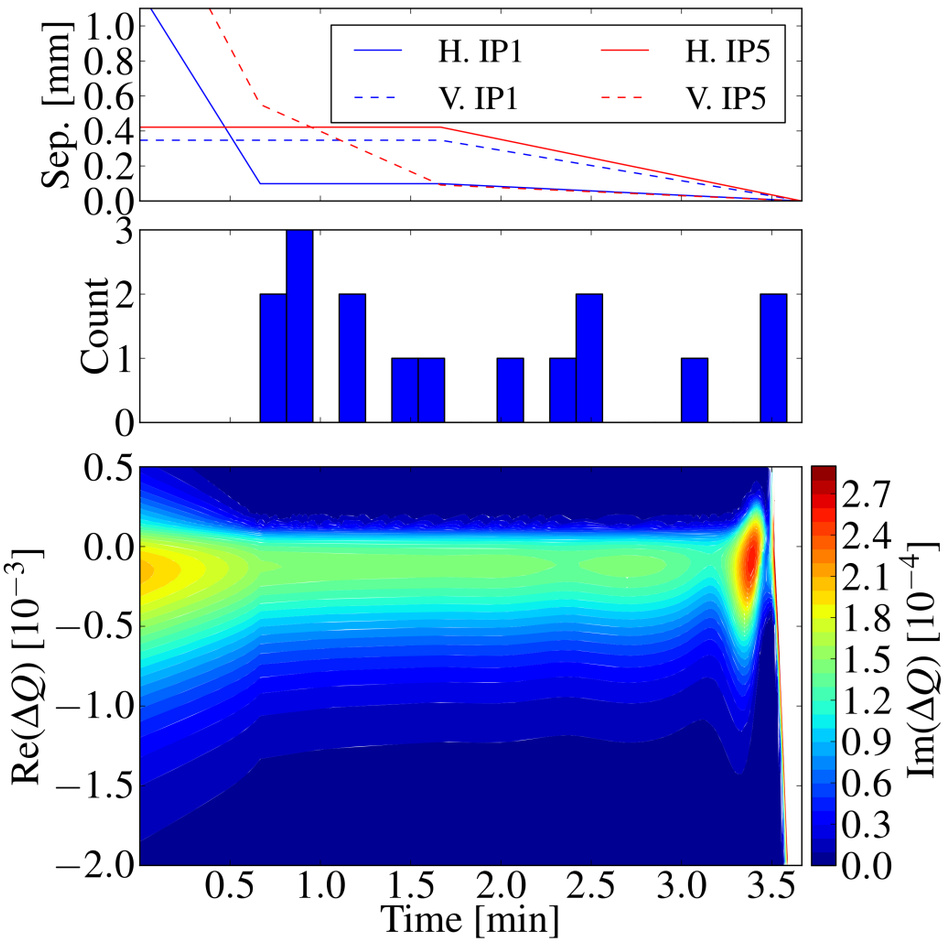

Figure 5: Illustration of the slow collapse of the separation bumps implemented in the first part of 2012 (top plot) starting with fully separated beams to the establishment of head-on collision. A significant amount of time was spent in a configuration where the stability diagram is reduced (bottom plot). The histogram of the instabilities observed when operating with the negative polarity of the octupoles shows that most of the instabilities occurred during this quasi-steady phase (middle plot). Such a slow collapse of the separation bumps was avoided in Run 2.

In the meantime several studies are ongoing to understand its cause and possibly mitigate it. The main topics of research are as follows:

- the improvement of the accuracy of the impedance model through the comparison of the expected observables with measurements [36],
- the developement of new beam dynamics models taking into account the impact of the machine noise on Landau damping [14, 15],
- the revision of the validity of the classical approach for Landau damping based on stability diagrams in the presence of a transverse damper [37].

The operational tool allowing for systematic correction of linear coupling, including slow drifts along the year, as well as corrections of the triplet non-linear errors were introduced in the third year of Run 2 (2017) [38]. In 2017 and 2018, the arc octupoles strength could be reduced by a factor about 2, whereas it needed to be kept at the maximum value in the previous years as instabilities were observed during orbit manipulations in the two main interaction regions with squeezed optics, suggesting an impact of non-linear errors in the triplets and/or long-range beam-beam interactions on a skew plane [35, 39].

2.2 Beams colliding long-range

Long-range beam-beam interactions generate an amplitude detuning similar to the arc octupoles powered with the positive polarity, i.e. linear with the transverse actions with positive and negative direct and indirect coefficients, respectively [40]. Yet, for long-range interactions the indirect coefficient is half the direct, as opposed to about 0.73 times for the arc octupoles (nominal optics) [10]. While an exact compensation can not be achieved, the interplay of these two components is favourable for Landau damping only when operating with the positive polarity of the arc octupoles and unfavourable otherwise [41, 42].

2.2.1 OPERATIONAL EXPERIENCE

In 2012, the unfavourable interplay between long-range interactions and the arc octupoles on Landau damping led to a reduction of the stability diagram at the end of the squeeze and during the collapse of the separation bumps with respect to non-squeezed beams at the end of the ramp, for which long-range interactions are weak. Instabilities leading to losses and eventually beam dumps were observed during the collapse of the separation. The corresponding stability diagrams are shown in Fig. 5. Two dumps occurred at the very end of the process, when the beams are colliding with a small offset. They will be discussed in the next section. The majority of the dumps occurred when the beams were colliding long-range only, in the unnecessarily long steady phase during which orbit manipulations were performed around IP8. Thanks to the large strength of the octupoles at 4 TeV, the expected coherent tune shifts remained well within the stability diagram in spite of the unfavourable interplay between long-rang interactions and the arc octupoles [43]. As discussed above, the effect of linear coupling is expected to have had a stronger impact on the beam stability in this configuration.

2.3 Beams colliding with an offset

When the two beams are brought in collision, the beam-beam force can no longer be accurately described by the first order detuning coefficients. We rather use the approach developed in [40] to obtain the detuning with amplitude:

$$\frac{\Delta Q_x(a_x,a_y)}{\xi} = -\frac{\beta}{2\pi a_x \sigma}\left\langle \Delta x'(a_x\sigma\sin(\phi_x), a_y\sigma\sin(\phi_y))\sin(\phi_x)\right\rangle_{\phi_x,\phi_y} \tag{2.1}$$

$$\frac{\Delta Q_y(a_x,a_y)}{\xi} = -\frac{\beta}{2\pi a_y \sigma}\left\langle \Delta y'(a_x\sigma\sin(\phi_x), a_y\sigma\sin(\phi_y))\sin(\phi_y)\right\rangle_{\phi_x,\phi_y}. \tag{2.2}$$

The beams were assumed round at the IP, with the optical β function and the corresponding beam size at the IP σ. The particle's oscillation amplitude in the two transverse planes a_x and a_y are normalised to the beam size. The average is performed over the betatron phases ϕ_x and ϕ_y. ξ is the beam-beam parameter defined as:

$$\xi = \frac{N r_0}{4\pi\varepsilon_n} \tag{2.3}$$

with N the bunch population, r_0 the proton classical radius and ε_n the normalised emittance. In order to account for the crossing angle, we may solve these integrals numerically, using Hirata's iterative method for the 6D beam-beam kick [44]. The amplitude detuning for different configurations of crossing angle and separation bumps are depicted in Fig. 6. The details of the corresponding evolution of the stability diagrams for the LHC nominal configuration, i.e. a synchronous collapse of the separation bumps in IPs 1 and 5 with a separation bump perpendicular to the crossing angle bump in each IP, were already discussed in [41]. In particular, the fact that the footprint *flips* for separations around 1.5σ (Fig. 6c) leading to a local minimum of Landau damping (Fig. 7b). We note nevertheless that the behaviour of the tail particles, highlighted with solid and dashed black lines on Figs. 6b, 6d and 6f differs significantly in each of the configurations. Whereas in the configuration without crossing angle we observe that the footprint width increases when decreasing the separation down to about 4σ, it then reduces to reach a minimum at a separation of approximately 2σ (Fig. 6b). Eventually the width increases again to reach its final value once the beams are colliding head-on. The presence of a crossing angle induces a flipping of the 'wings' of the footprint well visible in Fig. 6d. This occurs for Piwinski angle Φ_p above approximately 0.8:

$$\Phi_p = \frac{\sigma_s}{\sigma}(\theta + \theta_{CC}), \tag{2.4}$$

with σ_s the r.m.s. bunch length, θ the half crossing angle at the IP and θ_{CC} the crab angle.
The evolution of the stability factor during the process of bringing the beams into collision is shown in Fig. 7 for various octupole currents and for different configurations of separation bump, crossing angle bump and crab cavity powering. Similarly to [41], the amplitude detuning was obtained by tracking with MAD-X rather than using Eqs. 2.1 and 2.2. The octupoles current is varied outside of their capabilities to emulate an increase of the detuning coefficient using the ATS optics, which features increased β function at the arc octupoles [45]. Nevertheless, the modification of the ratio between the direct and indirect detuning term introduced by the ATS optics has an impact on Landau damping illustrated in Fig. 8 which is not taken into account here.
In most configurations we can identify two critical areas in terms of octupole current and parallel separation at IPs 1 and 5. The first corresponds to low octupole currents at large separations, this area extends mostly towards negative octupole currents due to the interplay of the tune spread generated by the arc octupoles and the ones generated by long-range beam-beam interactions. When collapsing the separation

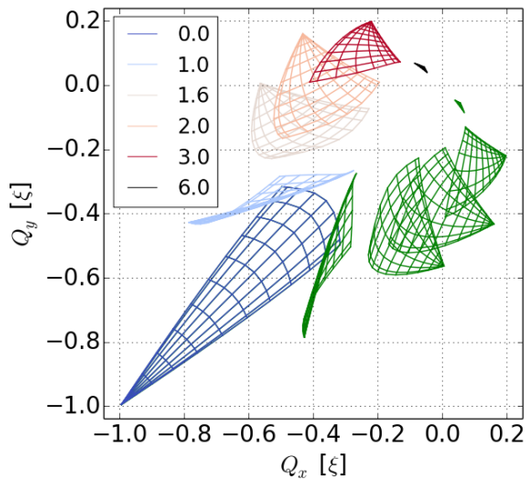

(a) Collapse of the separation bump in the horizontal plane (colors) or in the vertical plane (green) at one IP.

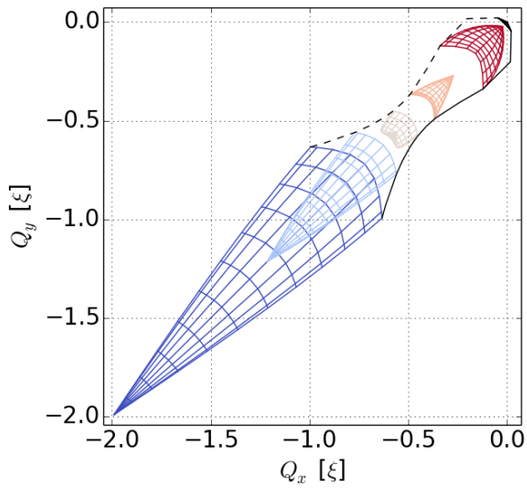

(b) Collapse of the separation bumps in two IPs with alternating separation planes.

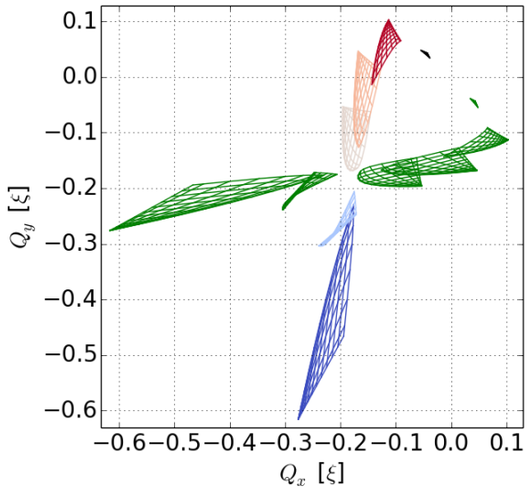

(c) Collapse of the separation bump in the horizontal plane (colors) or in the vertical plane (green) at one IP featuring a crossing angle in a plane perpendicular to the one of the separation bump. The Piwinski angle is 1.

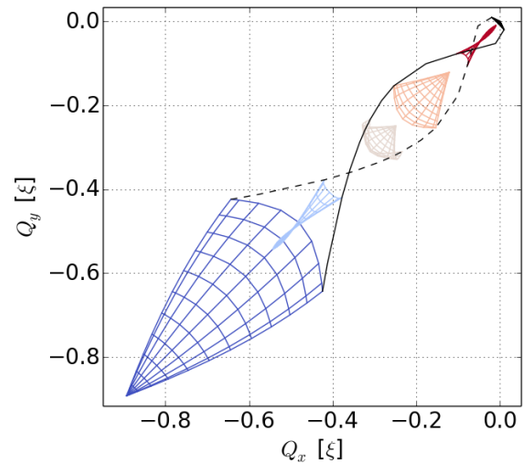

(d) Collapse of the separation bumps in the two IPs with alternating separation planes and featuring a crossing angle in the plane perpendicular to the one of the separation bump. The Piwinski angle is 1.

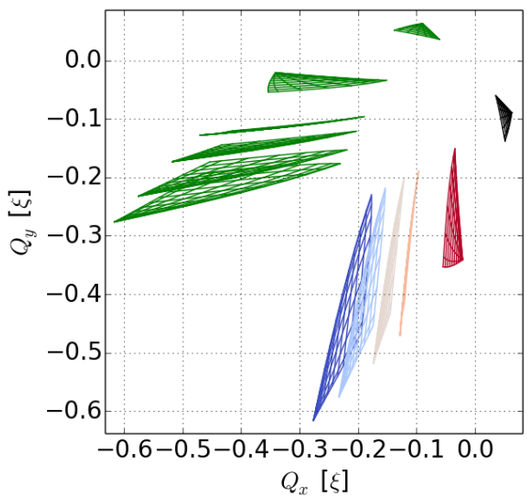

(e) Collapse of the separation bump in the horizontal plane (colors) or in the vertical plane (green) at one IP featuring a crossing angle in the same plane as the one of the separation bump. The Piwinski angle is 1.

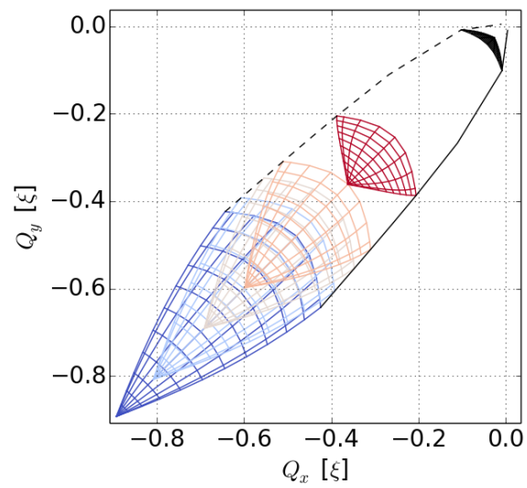

(f) Collapse of the separation bumps in the two IPs with alternating separation planes and featuring a crossing angle in the same plane as the one of the separation bump. The Piwinski angle is 1.

Figure 6: Tune footprint of particles oscillating at amplitudes meshing the transverse planes on a uniform polar grid with radii ranging from 0 to 3σ and angles ranging from 0 to 90° between the horizontal and vertical planes. The time evolution of the particles oscillating at 3σ in the horizontal plane during the process of bringing the beams into collision is marked with a black solid line, whereas the one of particles oscillating at 3σ in the vertical plane is marked with a black dashed line.

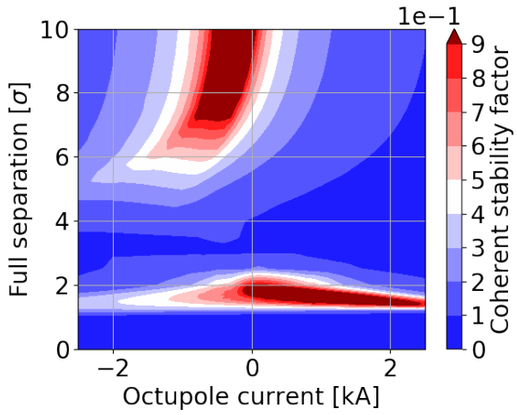

(a) Synchronous collapse of the separation bumps in IPs 1 and 5 with crab cavities disabled

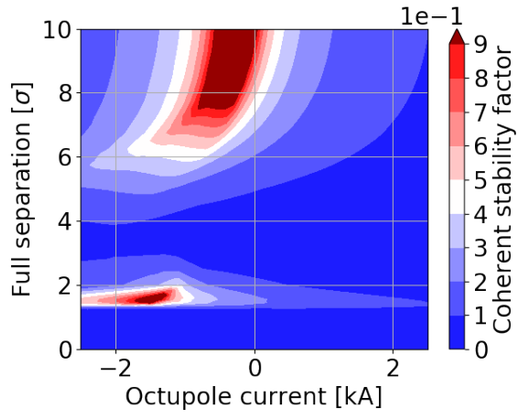

(b) Synchronous collapse of the separation bumps in IPs 1 and 5 with crab cavities partially compensating the crossing angle ($\phi_{CC} = -150\mu$rad)

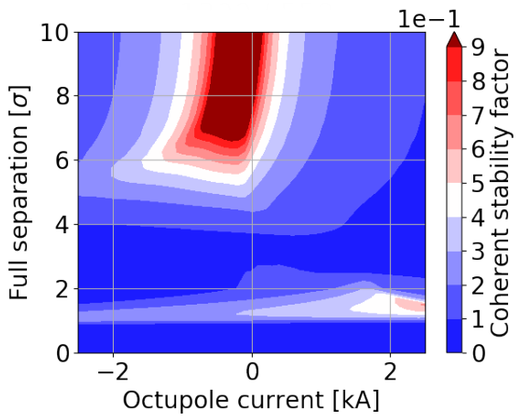

(c) Collapse of the separation bump in IP1 (vertical crossing angle) with crab cavities partially compensating the crossing angle ($\phi_{CC} = -150\mu$rad), stability factor in the horizontal plane

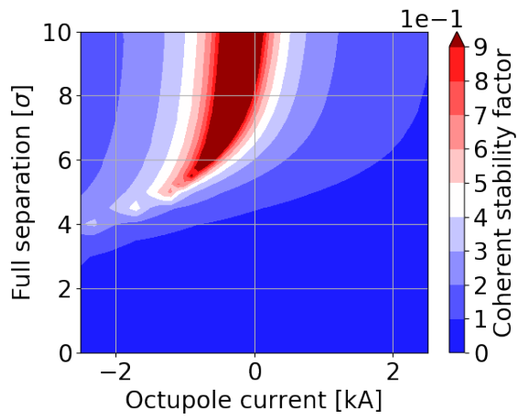

(d) Collapse of the separation bump in IP1 (vertical crossing angle) with crab cavities partially compensating the crossing angle ($\phi_{CC} = -150\mu$rad), stability factor in the vertical plane

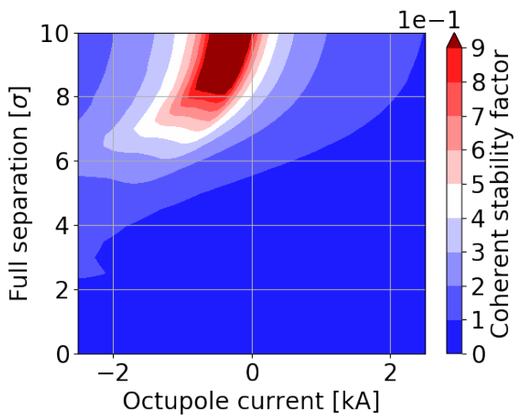

(e) Synchronous collapse of separation bumps in the crossing angle plane at IPs 1 and 5 with crab cavities disabled

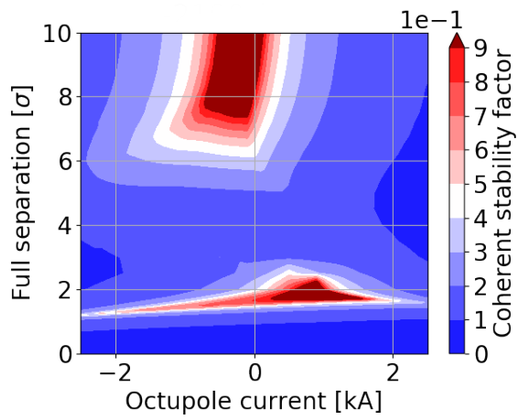

(f) Collapse of a separation bump in the crossing angle plane at IP1 (vertical crossing angle) with crab cavities disabled, stability factor in the vertical plane

Figure 7: Coherent stability factor as a function of the full normalised parallel separation between the beams at IPs 1 and/or 5 and octupole currents. The machine and beam parameters are those of the ultimate scenario with BCMS beams as described in [2], yet with $\beta^* = 1$m. The beams are fully separated at IPs 2 and 8. The stability factor is obtained by comparing the coherent tune shifts to the stability diagram obtained with PySSD [43] based on single particle tracking with MAD-X using the thin optics version 1.3 [23]. The coherent tune shifts were computed with DELPHI based on the baseline HL-LHC impedance model (Sec. 3.1). The separation bump is by default implemented in the plane perpendicular to the crossing plane. Unless the plane is specified, the stability factor is equal in both planes.

bumps synchronously in the two main IPs, this area extends further towards high negative currents when the separation is reduced until a separation of about 6σ. There are two contributors to this shift. The first is the increase of the strength of the long-range interactions when collapsing the separation bumps, which generates an additional separation between the beams mostly for the interactions in the drift space [43]. This contribution can be reduced by collapsing the separation bump in one IP at a time, i.e. in an asynchronous manner. Yet, in the HL-LHC the contribution of long-range interactions is rather weak at the start of collision thanks to luminosity levelling with β^*, therefore this strategy is not particularly helpful at this stage of the process. The second contribution comes from the single interaction at the IP, which is still comparable to a long-range interaction at this stage of the process. Collapsing the separation bump in one IP at a time helps in the plane of the separation, as can be observed by comparing Figs. 7b and 7c. Yet by comparing Figs. 7b and 7d, we observe that in the other plane the impact is marginal, such that the mitigation is rather ineffective as well.

The second critical phase is reached at separations of about 1.5 σ. This unstable area corresponds to a change of regime below which Landau damping is dominated by the contribution of the head-on interactions. In this intermediate regime, the tune footprint flips along the diagonal as the tune of particle oscillating with a small amplitude is shifted down, whereas the dynamics of particles oscillating with a large amplitude remains dominated by other forces, i.e. octupoles and long-range interactions. As a result, the contribution of low amplitude particles to Landau damping is canceled for separation around 1.5σ, therefore the amplitude detuning for the tails of the distribution must be sufficiently large to ensure Landau damping.
Similarly to the interplay between long-range interactions and the arc octupoles described above concerning the first unstable area, the minimum of stability is shifted to negative currents when the effective crossing angle at the IP is low ($\Phi_p < 0.8$), e.g. when the crab cavities are enabled for the collapse of the separation bump (Fig. 7b). On the other hand when the crab cavities are not enabled when collapsing the separation bumps, the unstable area is shifted to the positive octupole currents (Figs. 7a and 7b). This is due to the beam-beam force at the IPs with both a transverse offset and a crossing angle. As discussed above (Fig. 6d), this results in a flip of the tails of the footprint for separations between approximately 1.5 and 3σ which is highlighted with the solid and dashed black lines. Consequently the contribution of the beam-beam interaction compensates the arc octupoles when operated with the positive polarity in this intermediate phase only.
The second minimum of stability is fully lifted by introducing a separation bump in the same plane as the crossing angle bump, as observed in Fig. 7e. This occurs thanks to yet another behaviour of the tune footprint depicted in Fig. 6f. In this regime the contribution of the beam-beam interaction to the tail is rather large and the most critical compensation occurs only at very large negative octupole currents such that it should not be a concern for the HL-LHC configuration. This mitigation works effectively only when the collapse of the separation bumps is performed synchronously in both IPs. If not, the minimum of stability remains in the other plane (Fig. 7f). We note that in this configuration the longitudinal variations of the beam-beam force are rather large and their effect on Landau damping is neglected. One may expect that such variations will introduce additional Landau damping, yet the impact should be quantified by extending the analytical model or by means of tracking simulations. In addition, those longitudinal variations of the beam-beam force may generate mode coupling instabilities of colliding beam involving high order head-tail modes that are not efficiently suppressed by the damper [46]. They should also be studied in more detail.

The impact of these considerations on the operational cycle of the HL-LHC are discussed in Sec. 3.

2.3.1 Speed of the collapse of the separation bump

The speed of the collapse of the separation bump plays an important role in the execution of the cycle. Indeed, we identified two critical sets of separations that feature a strong reduction of Landau damping: first at separations around 6 σ for the negative polarity only and second at separations around 1.5σ for both polarities and depending on the configuration. The time evolution of the separation bumps is constrained by the relatively slow timescale of the superconducting magnets producing it. In particular, such small separations are reached towards the end of the process, during which the current ramp rate is slowly reduced to avoid voltage spikes. Taking into account these constraints, the reduction from 10 to 4 σ and from 2 σ to head-on collision can each be performed within less than 1 second [50]. This time is about twice the expected instability rise times [11, 12]. We note that the mode with the fastest growth rate is a coupled bunch mode driven by the crab cavity impedance in the vertical plane [12]. In absence of crab cavity impedance, the most unstable mode is twice as slow. Those estimates correspond to a total absence of Landau damping. Here we expect that Landau damping is not sufficient to stabilise the beam, yet it is not fully lost. Consequently the instability rise time are likely to be even longer. Instabilities will

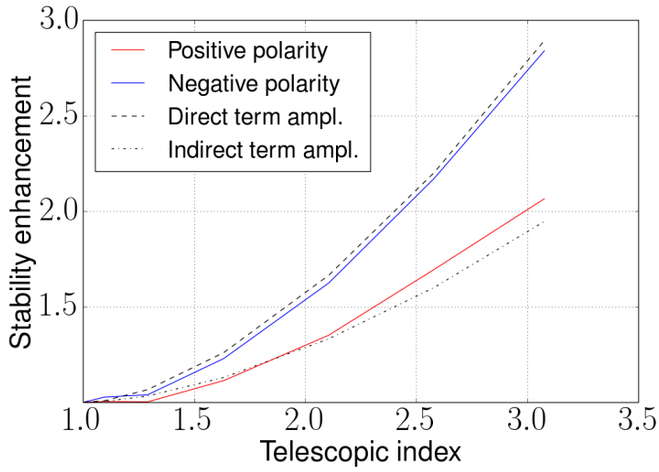

Figure 8: Enhancement of Landau damping for the two polarities of the octupole as function of the telescopic index. The enhancement is based on the comparison of the expected complex tune shifts obtained with DELPHI and the stability diagrams computed numerically with PySSD on MAD-X single particle tracking data using the 2018 optics for the round ATS MD [47] with various telescopic index. The expected enhancement of the direct and indirect detuning terms are shown in dashed and dotted lines respectively [48]. The details of the shape of the stability diagram are discussed in [49].

therefore not have the time to develop in these transient phases. The reproducibility of the orbits and of the separation bumps has to be sufficient to ensure that the end point of the process corresponds to a full separation lower than $\approx 1\sigma$. This would be challenging if collision had to be established at low β^* but seems within reach thanks to the establishment of collision at a higher β^* [51].
The reduction of Landau damping with offset beams remains a concern for steady configurations for which a separation is needed, e.g. during luminosity levelling with transverse offsets by a factor larger than $\approx 20\%$ or during Van der Meer-like scans in physics conditions (also known as emittance scans). For the latter, a loss of Landau damping can be avoided by performing the emittance scan in one of the main IP maintaining the other head-on during the procedure.

2.4 Operational experience

In 2012, two instabilities leading to beam dumps during the collapse of the separation bumps can be attributed to the reduction of the tune spread with beams colliding with a small offset, as shown in Fig. 5. Also, several instabilities were observed due to luminosity levelling with a transverse offset in IP8. This instability affected few bunches colliding in this IP only, whereas most of the bunches were colliding head-on in the two main IPs and were stabilised by their large contribution to Landau damping. These instabilities occurred when operating with the negative polarity of the octupoles [52] and a transverse separation about 1.5σ [41]. As the Piwinski angles were rather small in all IPs in 2012 ($\Phi_p < 0.8$), the negative polarity is indeed more critical, similarly to the case with crab cavities enabled discussed above.
In 2017 instabilities linked to collisions with a small transverse offset were observed during Van der Meer scans while operating with the positive polarity of the octupoles. The octupoles current was in fact set too low in an attempt to reduce tail population [53].
In 2017 and 2018, a set of controlled experiments with offset beams confirmed the existence of the loss of Landau damping of beams colliding with a transverse offset of approximatively 1.5σ for a range of octupole currents [47, 54]. In addition, it was shown experimentally that the instability is observed only when several tens of seconds are spent at the critical separation, whereas the instability is fully suppressed by collapsing the separation bumps at the maximum speed, thus crossing the unstable configuration rapidly [47].

3 Strategy for the HL-LHC cycle

In the following we discuss the consequences of the choice of polarity of the arc octupoles on the HL-LHC cycle assuming that it has to remain fixed through the cycle, including luminosity production. Then, the possibility to decouple the choice of polarity during the cycle and during luminosity production by flipping the polarity when the beams are colliding is discussed.

	CFC	Baseline	Retracted
Oct. thres. [A]	820	550	460
Equi. teleindex	2.3	1.0	1.0

(a) Positive polarity

	CFC	Baseline	Retracted
Oct. thres. [A]	-2100	-1540	-1350
Equi. teleindex	3.6	2.9	2.7

(b) Negative polarity

	CFC	Baseline	Retracted
Oct. thres. [A]	-1070	-873	-718
Equi. teleindex	2.5	2.0	1.7

(c) Negative polarity with the assumption that Landau damping can be lost for a transient shorter than the instability rise time in ADJUST (Sec. 2.3.1).

Table 1: Stabilising octupole current together with the teleindex required to reach the equivalent detuning coefficient when operating the octupoles at the maximum of their capacity. The optics V1.3 was used with a β^* of 1 m and a crossing angle of 250μrad in all cases. The other parameters are those of ultimate scenario with BCMS beams [2]. For the positive polarity (upper table) the most stringent limit is for a single beam (without beam-beam interactions) at the end of the ramp or squeeze. For the negative polarity (middle table), the configuration with synchronous collapse of the separation bumps and crab cavities off at the start of collision was considered (Fig. 7a). Assuming that Landau damping can be lost transiently during ADJUST (bottom table), the same configuration was considered but the most stringent limit is now evaluated at a full separation between the beams at the IP of 10σ.

3.1 Impedance model

In the following we will consider the latest revision of the impedance model for the HL-LHC including in particular the crab cavities and the low impedance upgrade of the collimators [12, 13]. The collimator upgrade consists mainly in the replacement in IR7 and in each beam of 2 out of 3 primary collimators (TCPs) and 9 out of 11 secondary collimators (TCSGs) by new ones featuring Molybdenum-Graphite jaws. Additionally, the 9 upgraded seconday collimators are coated with Molybdenum [11, 55, 56]. The details of the collimator settings are described in [12]. This model will be quoted as the **Baseline** scenario. We also consider two variations of the this model.

- In the **CFC** scenario, the low impedance collimators are replaced by old collimators featuring Carbon Fiber-reinforced Carbon (CFC) jaws. The comparison of the results obtained with this model with respect to those obtained with the baseline scenario allows to quantify the impact of the collimator upgrade.
- In the **Retracted** scenario, the gaps are increased in the primary collimators from 6.7 to 8.5 σ and in the secondary collimators from 9.1 to 10.1 σ. Other absorbers, tertiary as well as IR6 collimators are slighlty retracted with a minor impact on the impedance [57]. This scenario is interesting to quantify the potential of a retraction of the collimator hierarchy to improve the beam stability.

3.2 Positive polarity

The main benefit of the positive polarity is the favourable interplay with the long-range beam-beam interactions for Landau damping. In this regime, the stability is the most critical in two configurations. First at the end of the ramp, when the effect of long-range beam-beam interaction is the weakest. In the ultimate scenario, the betatron squeeze results in an increase of the tune spread. A second critical point is reached when bringing the beams into collision if the Piwinski angle is large. As discussed in Sec. 2.3, the effect of the interaction at the IP with a large Piwinski angle and a transverse offset can result in a loss of Landau damping. This effect is visible in Figs. 9b, 9d and 9h as a wide range of parameters lead to stabilising beam currents above 2.3 kA (or equivalently large telescopic index) which are not reachable. The only suitable parameters feature a low Piwinki angle (large β^* and/or crab angle compensating a large fraction of the crossing angle). The loss of Landau damping at separations $\approx 1.5\sigma$ is well mitigated by introducing a separation bump parallel instead of perpendicular to the crossing plane (Sec. 2.3). Its effectiveness is clearly visible in Fig. 9f, as the stabilising octupole current is the lowest for any choice of β^* and crab angle in the range considered. On the other hand the mitigation is not as effective if the separation bump is collapsed in one IP at a time (Fig. 9h), as the loss of Landau damping is mitigated in the plane perpendicular to the crossing plane only. The stability therefore remains as critical in the other

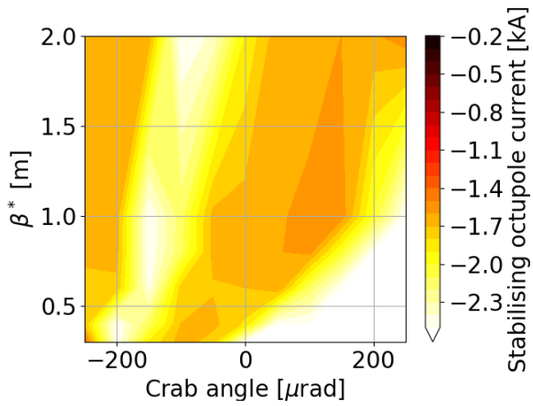

(a) Synchronous collapse of IP1 and IP5 separation bumps perpendicular to the crossing plane ($I_{oct} < 0$).

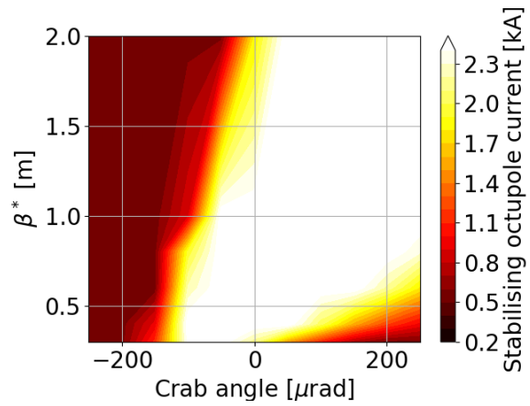

(b) Synchronous collapse of IP1 and IP5 separation bumps perpendicular to the crossing plane ($I_{oct} > 0$).

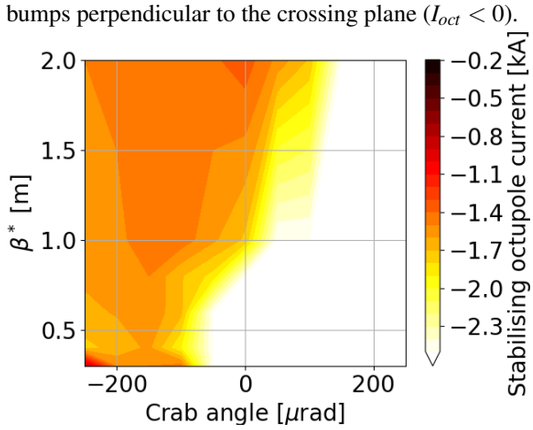

(c) Collapse of IP1 separation bump perpendicular to the crossing plane ($I_{oct} < 0$).

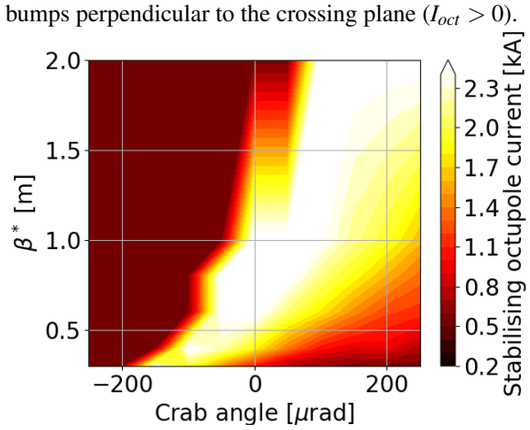

(d) Collapse of IP1 separation bump perpendicular to the crossing plane ($I_{oct} > 0$).

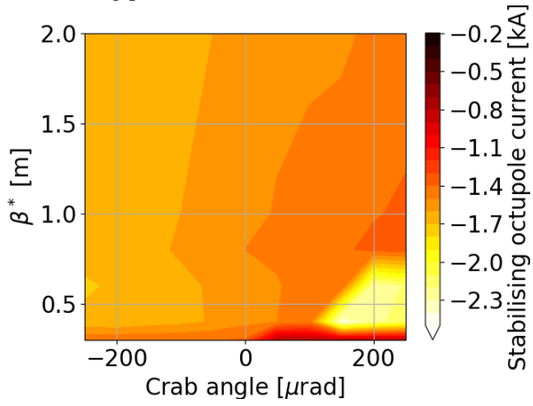

(e) Synchronous collapse of IP1 and IP5 separation bumps parallel to the crossing plane ($I_{oct} < 0$).

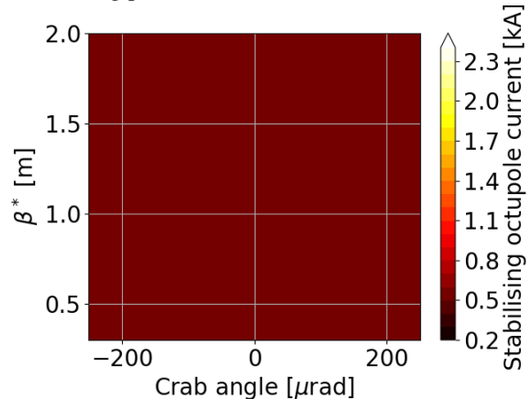

(f) Synchronous collapse of IP1 and IP5 separation bumps parallel to the crossing plane ($I_{oct} > 0$).

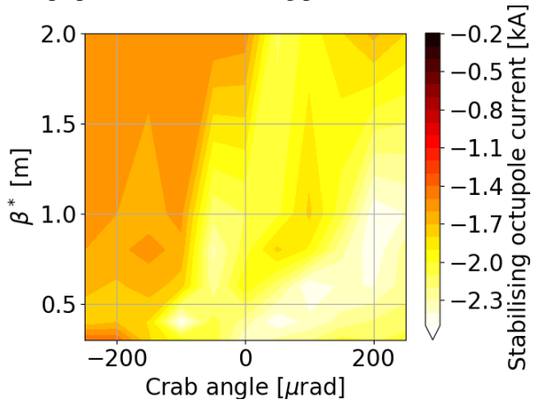

(g) Collapse of IP1 separation bump parallel to the crossing plane ($I_{oct} < 0$).

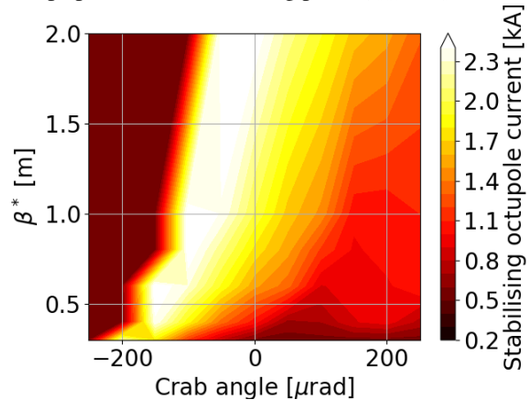

(h) Collapse of IP1 separation bump parallel to the crossing plane ($I_{oct} > 0$).

Figure 9: Minimum stabilising octupole current over the cycle as a function of the crab angle and β^* at the start of collision. The beams are fully separated at IPs 2 and 8 when the separation bumps are collapsed. The stability factor is obtained by comparing the coherent tune shifts to the stability diagram obtained with PySSD [43] based on single particle tracking with MAD-X using the thin optics version 1.3 [23]. The coherent tune shifts were computed with DELPHI based on the baseline HL-LHC impedance model (Sec. 3.1). The other machine and beam parameters are those of the ultimate configuration with BCMS beams [2]. On the horizontal axis, the crab angle is defined such that it adds to the crossing angle of 250 μrad. Consequently, a negative crab angle corresponds to a compensation of the crossing angle.

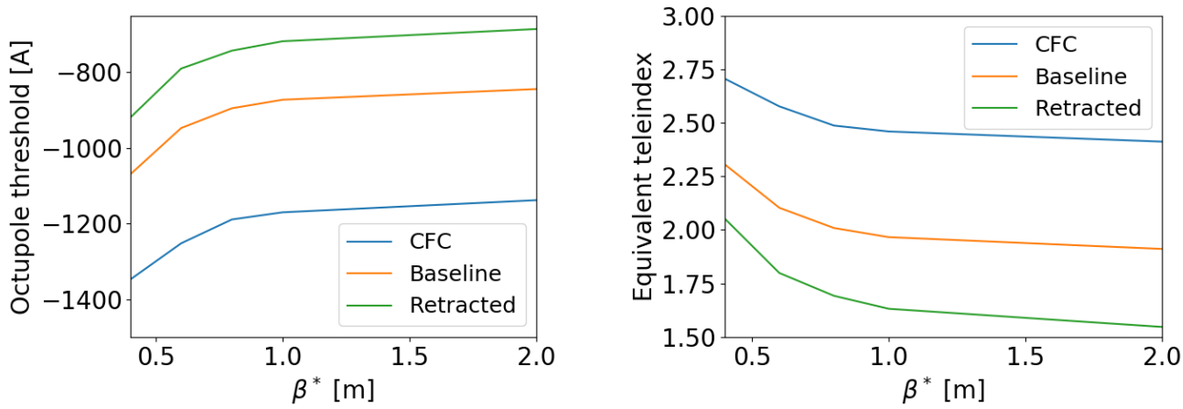

(a) (b)

Figure 10: Stabilising octupole current during the collapse of the separation bump at a full separation between the beams at the IP of 10σ for different β^*. The corresponding teleindex required to reach the equivalent detuning coefficient when operating the octupoles at the maximum of their capacity is shown on the right. The optics V1.3 was used and the half crossing angle was set to 250μrad. The other machine and beam parameters are those of ultimate scenario with BCMS beams [2].

plane.

There are two alternatives to the implementation of a separation bump in the crossing plane. First the collapse of the separation bump in one IP at a time with the crab cavities enabled (Fig. 9d) or relying on the speed of the collapse of the separation bump (Sec. 2.3.1). In all these options the strict minimal requirement is given by the stability in absence of beam-beam interactions. Those stability limits for the difference scenarios are listed in Tab. 1a. In absence of low impedance collimator upgrade (CFC scenario) a significant telescopic index is needed at the end of the ramp to boost the effectiveness of the octupoles. The baseline scenario is at the edge of the capacity of the octupoles of 570 A, consequently it does not leave margin for the compensation of machine imperfections. This aspect will be detailed in Sec. 3.4.

We note that in general increasing the crossing angle is not helpful when operating with the positive polarity of the octupoles since the interplay with long-range interaction is favourable for Landau damping. On the contrary, large Piwinski angles are detrimental at small separation between the beams at the IP, therefore a reduced crossing angle is favourable, within the limits imposed by the effect of the non-linearity of the long-range interaction on the long term stability of single particle trajectories. Colliding at the largest β^* is also favourable in all configurations limited by the loss of Landau damping at $\approx 1.5\sigma$ as it reduces the Piwinski angle.

For Van der Meer scans or other types of separation scans, it is required to introduce an offset in both planes and remain steady with the beams separated for times longer than the expected instability rise time. As shown in Fig. 9d, instabilities can be expected for certain choices of β^* and crab angle. As mentioned above, a large β^* is favourable for beam stability. If nevertheless such separation scans should be performed in these conditions, another IP must be maintained in collision to provide sufficient Landau damping.

3.3 Negative polarity

The interplay of the arc octupoles with the beam-beam interactions is in general less favourable when operating with the negative polarity. It is clearly visible in Fig. 9, as all configurations require less than the -570 A achievable by the arc octupoles. As for the positive polarity, the implementation of a separation bump in the crossing plane is the most favourable option in terms of flexibility (Fig. 9e). We report in Tab. 1b the requirements at $\beta^* = 1$ m without crab cavity. In this configuration an increase of the crossing angle and/or of the crab angle, i.e. operating the crab cavities enhancing the crossing angle at the IP instead of compensating it, can reduce the requirement by up to 10%. The maximum of the reduction is based on the largest crab angle that can be achieved with the crab cavities (180 μrad) and increasing the crossing angle to the highest value compatible with the orbit correction scheme (295 μrad [58]). Such an improvement does not lift the need for a significant telescopic index to boost the efficiency of the arc octupoles. Consequently, the operation with the negative polarity will have to rely on the execution of the collapse of the separation bump with a sufficiently high speed, such that transient phases featuring a loss of Landau damping are significantly shorter than the instabilty rise time. This prevents the developement

β^* [m]	Bare machine	b4 with corr.	b4 with corr. +ab56 w/o corr.	b4 with corr. +ab56 with corr.	b4 with corr. +ab56 with corr. +higher orders w/o corr.
3.00	4	2	-8		
0.64	-5	9	52	15	14
0.41	-10	20	125	33	34
0.15	-98	178	903	229	251

(a) Direct

β^* [m]	Bare machine	b4 with corr.	b4 with corr. +ab56 w/o corr.	b4 with corr. +ab56 with corr.	b4 with corr. +ab56 with corr. +higher orders w/o corr.
3.00	-13	-16	-27		
0.64	-27	-19	-47	-24	-24
0.41	-46	-34	-108	-45	-51
0.15	-235	-221	-837	-318	-369

(b) Indirect

Table 2: Amplitude detuning expressed in terms of equivalent impact of the Landau octupoles power with a given current on the direct and indirect amplitude detuning, without telescopic index. The contribution of the bare machine as well as the cumulative effect of the other contributions is shown: The amplitude detuning left after correction of the b4 components in the IR with dedicated correctors, the feed down from the decapole and dodecapole components of the triplets (a5, b5, a6 and b6) with and without dedicated beam-based correction as well as higher order components for which no correction scheme is planned. The error model is based on WISE [59], the results shown here correspond to the worst of 60 random seeds for each combination of the sources. The HL-LHC optics V1.3 [23] was used.

of the instabily and the corresponding deteriorations of the beam quality (Sec. 2.3.1). In this case, the most stringent limit for the octupole requirement is still during the collapse of the separation bumps, but for the lengthy process from a total separation of several tens of σ to about 10 σ. In this phase, Landau damping is dominated by the interplay of the arc octupoles and the parasitic long-range interactions. The long-range interactions are the strongest at the end of the process as the combination of the crossing and separation bumps increases the distance between the beams in the triplets and the drift space. In Tab. 1c we report the octupole requirement at a separation of 10 σ, which now represents the minimum requirement through the cycle. As opposed to the positive polarity, the minimum octupole strength required with the negative polarity depends on the strength of the parasitic long-range interactions. The estimates in Tab. 1c correspond to a normalised separation of 33 σ in the drift space. The increase of the required current, as well as the equivalent teleindex, when reducing β^* at a fixed crossing angle is shown in Fig. 10. At the smallest β^* considered (40 cm), the normalised separation is 21 σ. The required teleindex reaches 2.3 with the baseline collimator settings and 2.1 with the retracted collimators.

We note that first experimental tests at the LHC introducing a large telescopic index (3.1) during the ramp did not exhibit major difficulties, in particular the reduction of the required octupole current was demonstrated [47, 48].

Similarly to the positive polarity, the range of β^* and crab angle for which the stability can be maintained is limited for slow separation scans such as Van-der-Meer or emittance scans (Figs. 9c and 9h). Again, stabilisation by the Landau damping generated by a head-on beam-beam interaction at another IP is a possible mitigation.

3.4 Non-linear optics correction

The estimations of the requirements in terms of octupole strength and telescopic index do not account for margins for other contributions to the amplitude detuning. The details of the main contributors are shown in Sec. B. Tables 2a and 2b describe the worst contributions to the indirect and direct terms respectively, expressed relatively to the contribution of the arc octupoles with a given current and for a telescopic index of 1. Since the strength of Landau damping for coherent modes with negative tune shifts is dominated by the direct and indirect terms for the negative and positive polarity respectively, the worst contribution is either the most positive (Tab. 2a) or the most negative (Tab. 2b). The contribution of the bare machine, dominated by the second order effect of the sextupoles for chromatic correction, is already included in the estimations above.
The distribution of the residual detuning for different random errors are shown in Fig. 11 for the most

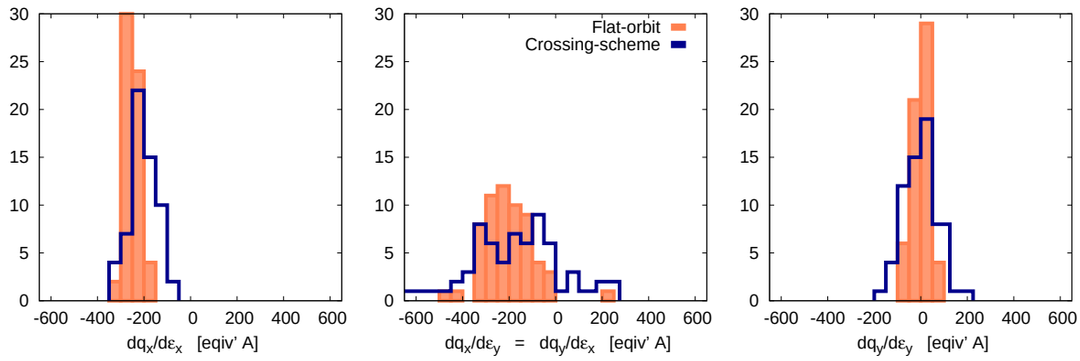

Figure 11: Distribution of the residual linear detuning terms for 60 different random error seeds based on WISE [59] for the HL-LHC optics v1.3 with a β^* of 15 cm. The contribution of the lattice sextupoles is included.

	$I_{oct} > 0$		$I_{oct} < 0$	
	I_{oct} [A]	r_{ATS}	I_{oct} [A]	r_{ATS}
Baseline	520	1.4	-555	2.1
Retracted	460	1.0	-548	1.8

Table 3: Minimal octupole current and telescopic index required at flat top and during the squeeze in the best configuration described in Tabs. 1a and 1c for both polarities of the octupoles. The teleindex is chosen such that there is enough margin with respect to the maximum current of the octupole ($\pm 570A$) to compensate for uncorrected linear coupling and triplet non-linearities using the lattice octupoles for $\beta^* > 64$ cm.

extreme configuration in terms of non-linear errors, i.e. with a β^* of 15 cm. We note in particular the high sensitivity of the residual indirect term on the exact error model.
When operating with the positive polarity of the octupoles, we find in Tab. 2b that an additional current up to 24 A might be required to compensate for the impact of the non-linear errors on the indirect detuning terms for $\beta^* = 64$ cm or higher. In addition to the non-linear errors, we require that the detrimental effect of linear coupling can be compensated by an additional strength of the arc octupoles. As discussed in Sec. 4, it is possible to maintain a tune separation of at least 0.01 during the squeeze, such that the detrimental effect of linear coupling is kept under 4% for linear coupling corrected under $\Delta Q_{min} < 10^{-3}$. These contributions sum up to a maximum of -43 A. In order to allow for such a compensation, a teleindex of 1.4 allows for a reduction of the threshold to 520 A, thus leaving enough margin to compensate for the impact of lattice imperfections if needed. When considering the configuration with retracted collimators, the teleindex is not required. These results are summarised in Tab. 3.
For the negative polarity Landau damping is dominated by the direct term. Equivalently we find on Tab. 2a that an additional-14 A may be required from the arc octupoles to compensate for the other contributions to amplitude detuning at $\beta^* = 64$ cm. As opposed to the configuration with the positive octupole polarity, the most critical point in the cycle in terms of Landau damping is during the collapse of the separation bump. As discussed in Sec. 4, the tune separation in this configuration needs to be reduced to about $5 \cdot 10^{-3}$. With a correction of linear coupling such that $\Delta Q_{min} < 10^{-3}$, the strength of the arc octupoles might have to be increased by up to 4% to maintain Landau damping. The estimated increase of the telescopic index and the recommended octupole current are summarised in Tab. 3.

The contributions of non-linear errors to amplitude detuning are exacerbated at low β^*. Thanks to the large telescopic index required to reach $\beta^* = 15$ cm, these contributions may still be compensated by the arc octupoles in order to maintain the stability of non-colliding bunches. This scheme might however not be optimal for the dynamic aperture and a compromise between the brightness of the non-colliding bunches and the full beam lifetime might have to be made. A significant reduction of the brightness of the non-colliding bunches is considered acceptable if needed to optimise the integrated luminosity [60, 61].

3.5 Polarity flip in collision

The stability requirements for the cycle and the production of luminosity are significantly different, due to the presence of head-on beam-beam interactions in the latter, dominating the contribution to Landau damping by inducing a large amplitude detuning for particles oscillating at small amplitudes, i.e. the core of the beam distribution. In this configuration, the contribution of long-range beam-beam interac-

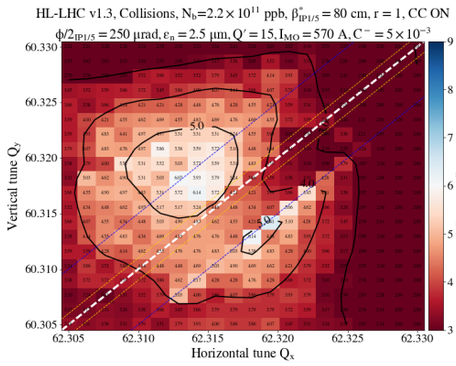

(a) Positive octupole polarity, CC enabled, teleindex 1.0

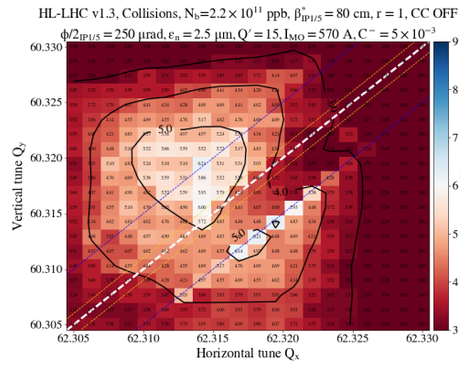

(b) Positive octupole polarity, CC disabled, teleindex 1.0

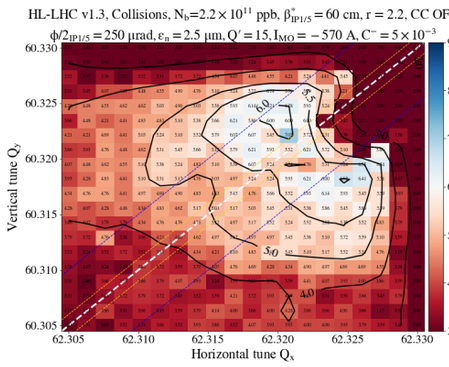

(c) Negative octupole polarity, CC disabled, teleindex 2.2

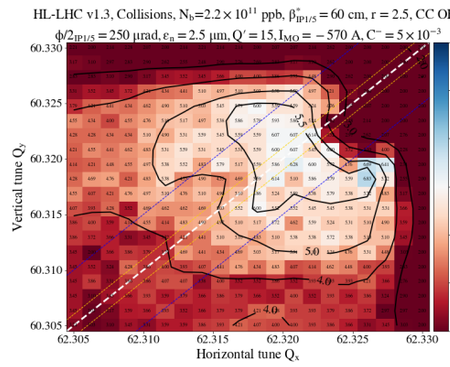

(d) Negative octupole polarity, CC disabled, teleindex 2.5

Figure 12: Dynamic aperture simulations based on Sixtrack [62] using the HL-LHC optics V1.3 [23] with beam-beam interactions in all interactions points and without magnetic errors [63]. Linear coupling was introduced using the skew quadrupole correction scheme, it strength was pessimistically set to $|C^-| = 5 \cdot 10^{-3}$. The machine and beam parameters are those of the ultimate HL-LHC scenario [2] unless specified in the captions. We note that, in previous estimates of coherent stability, the emittance is pessimistically assumed constant at 1.7 μm. Here the estimate is also chosen on the pessimistic side, with the design emittance of 2.5 μm in collision.

tions and the arc octupoles to Landau damping is no longer required. Moreover, as both the octupoles and the long-range interactions mainly impact the dynamics of particles oscillating at large amplitude, their contributions to Landau damping hardly interfere with the one of the head-on interactions. The choice of polarity and strength is therefore no longer constrained by coherent stability requirement, but can be varied to optimise single particle stability, i.e. beam lifetime. In particular, the favourable interplay between the long-range interaction and the arc octupoles with the positive polarity on the amplitude detuning, i.e. Landau damping, is on the other hand detrimental for dynamic aperture. In order to profit from both, a polarity reversal is required. This process does not affect the stability of colliding bunches, however the non-colliding bunches will necessarily go through unstable conditions. With the current ramp rate specification [50], the polarity flip requires slightly less than 4 minutes, an increase of the ramp rate by almost two orders of magnitude is required to reach flipping times comparable to the expected instability rise times. Nevertheless, we note that first experimental tests at the LHC suggest that the impact of such a polarity swap on the brightness of the non-colliding bunches remains minor [47]. Given that the brightness of the non-colliding bunches may be set significantly lower than the other bunches, since they serve a difference purpose [60, 61], we may expect that their degradation during an octupole polarity swap can be kept under control. If needed, the procedure for the polarity swap may be improved in various ways to maintain Landau damping for the non-colliding bunches. For example this can be achieved by acting differently on the direct and indirect detuning terms, such that they are not zero simultaneously. An example of such a procedure using the triplet octupole correctors (MCOX) is discussed in Sec. A.

4 Dynamic aperture

To avoid performance limitations one needs to minimise the particle diffusion from the beam core to the halo, which can be assured as long as the simulated dynamic aperture remains above 6σ with beam-beam interaction and magnet non-linearities [63]. The dynamic aperture is most critical in collision, in

the presence of strong beam-beam interactions. As discussed in Sec. 3.5, the octupole current can be adjusted to maximise the beam lifetime once in collision, within the limit imposed by the non-colliding bunches. Nevertheless, the stabilising effect of the head-on interactions is established only within the last second of the collapse of the separation bumps. This time does not allow for any significant variation of the machine parameters affecting the dynamic aperture (e.g. octupole current, chromaticity) in this phase. Consequently, the dynamic aperture should be sufficiently large at the start of collision with an octupole current and teleindex meeting the requirements for beam stability (Tab. 1).

Figure 12 shows the result of simulations at the end of the collapse of the separation bumps. For the positive polarity (Figs. 12a and 12b), a single set of tunes featuring a dynamic aperture above 6σ was found when operating the octupoles at maximum strength, without telescopic index. This is compatible with the requirements listed in Tab. 1a for the baseline collimator settings as well as for the retracted scenario. Nevertheless, the baseline configuration without teleindex does not leave any margin to compensate for lattice errors, whereas the retracted scenario offers enough margin without having to increase the teleindex (Tab. 3).
A single set of tunes can also be found when operating the octupoles at maximum strength with the negative polarity with a telescopic index of 2.5 (Fig. 12d). The situation is slightly more relaxed with a teleindex of 2.2 (Fig. 12c). Consequently, the requirements to maintain Landau damping at all stage of the cycle are not compatible (Tab. 1b). The only option for the negative polarity is therefore to transiently cross a loss of Landau damping during ADJUST (Sec. 2.3.1). In this case, the requirements for both the baseline and retracted scenario for the collimators can be met with the negative polarity (Tab. 1c), also including lattice errors (Tab. 3).

5 Conclusion

The positive polarity of the octupoles appears as a robust choice for the beam stability, since the interplay of the arc octupoles with beam-beam interaction is favourable for Landau damping in all configurations except for beams colliding with an offset at the IP and a large Piwinksi angle. This specific situation may occur in the HL-LHC when bringing the beams into collision with crab cavities off. It can be avoided simply by enabling the crab cavities before bringing the beams into collision. Alternatively (e.g. due to unavailability of the crab cavities or issues with crab cavity noise on non-colliding beams [64]), since the beams are expected to stay in this transient unstable configuration for a duration shorter than the fastest instability rise time, the instability can not grow significantly and consequently does not impact the beam quality. An additional mitigation of this transient loss of Landau damping could be envisaged using a separation bump in the crossing angle plane. We note that in the case Van der Meer scans need to be performed without crab cavities, a head-on collision would have to be maintained at another IP to ensure Landau damping.

The negative polarity was the initial choice for the LHC based on single beam stability considerations [16]. Later, the unfavourable interplay with long-range beam-beam interactions on Landau damping seemed responsible for severe stability issues in the first part of 2012 leading to beam dumps, based on considerations on the tune spread [42]. This effect is however not sufficient to fully explain the instability [41], whereas the lack of control on linear coupling was later identified as more critical and in quantitative agreement with the observations [24]. Thus it is not expected that issues similar to those observed in 2012 will appear when operating with the negative polarity of the octupole provided that the detuning generated by the arc octupoles is sufficient to compensate the effect of long-range interactions and that linear coupling as well as other lattice errors affecting the tune spread, such as the triplet non-linearities are accurately corrected. Such a control of the tune spread is required independently of the octupole polarity.
The negative polarity requires an increase of the strength of the octupole to compensate for the detrimental interplay with long-range beam-beam interactions and the offset interaction at the IP during the collapse of the separation bumps. This can be achieved using the ATS optics to boost the efficiency of the arc octupoles via an increase of the β function at their locations. This possibility was tested experimentally in the LHC providing encouraging results [48]. Nevertheless as opposed to the LHC test, the boost required to fully avoid a transient loss of Landau damping in the HL-LHC would lead to an unaccaptable reduction of dynamic aperture. If the initial β^* is sufficiently high, a lower teleindex can be found which yields an acceptable dynamic aperture and meets the requirements to maintain Landau damping through the cycle except during a short transient when the beams are brought into collision. Due to its short duration, this transient loss of Landau damping is not expected to impact the beam quality. For lower initial β^*, the required teleindex is larger due to the increased strength of long-range beam-beam interactions. In particular at an initial β^* of 40 cm, the requirements for Landau damping

can not be met without jeopardising the dynamic aperture, only the retracted scenario remains acceptable.

Both polarities of the octupoles seem acceptable for the operation of the HL-LHC with different constraints. The solid operational experience acquired with the positive polarity in Run 2, the reduced need for telescopic optics before collision and the additional flexibility for offset levelling slightly favour the positive polarity. Nevertheless the octupole polarity also affects the performance of the collider via its impact on the dynamic aperture in collision [25, 65, 66]. If found desirable, no show stopper was identified to operate the HL-LHC with the negative polarity. A polarity reversal in collision could also be considered in that case. This procedure was successfully tested experimentally [47].

References

[1] G. Apollinari, I. Béjar Alonso, O. Brüning, P. Fessia, M. Lamont, L. Rossi, and L. Tavian, *High-Luminosity Large Hadron Collider (HL-LHC): Technical Design Report V. 0.1*, CERN Yellow Reports: Monographs (CERN, Geneva, 2017).

[2] E. Métral, S. Antipov, F. Antoniou, R. Appleby, G. Arduini, J. Barranco, P. Baudrenghien, N. Biancacci, C. Bracco, R. Bruce, X. Buffat, R. Calaga, L. Carver, M. Crouch, R. D. Maria, S. Fartoukh, D. Gamba, M. Giovannozzi, P. Gonçalves Jorge, W. Hofle, G. Iadarola, N. Karastathis, A. Lasheen, K. Li, T. Mastoridis, L. Medina, A. Mereghett, D. Mirarchi, B. Muratori, S. Papadopoulou, Y. Papaphilippou, D. Pellegrini, T. Pieloni, S. Redaelli, G. Rumolo, B. Salvant, E. Shaposhnikova, M. Solfaroli, C. Tambasco, R. Tomàs, and D. Valuch, *Update of the HL-LHC Operational Scenarios for Proton Operation*, CERN-ACC-NOTE-2018-0002 (CERN, Geneva, Switzerland, 2018).

[3] N. Mounet, "Vlasov solvers and macroparticle simulations," in *ICFA Mini-Workshop on Impedances and Beam Instabilities*, Benevento, Italy, 18-22 Sep. 2017, edited by V. Brancolini, G. Rumolo, M. Masullo, and S. Petracca (CERN, Geneva, Switzerland, 2018) pp. 77–85.

[4] J. S. Berg and F. Ruggiero, *Landau damping with two-dimensional betatron tune spread*, SL-96-071-AP (CERN, Geneva, Switzerland, 1996).

[5] M. Schenk, X. Buffat, L. R. Carver, R. De Maria, K. Li, and E. Métral, "Experimental stabilization of transverse collective instabilities in the lhc with second order chromaticity," Phys. Rev. Accel. Beams **21**, 084401 (2018).

[6] M. Schenk, X. Buffat, K. Li, and A. Maillard, "Vlasov description of the effects of nonlinear chromaticity on transverse coherent beam instabilities," Phys. Rev. Accel. Beams **21**, 084402 (2018).

[7] L. Landau, "On the vibrations of the electronic plasma," J.Phys.(USSR) **10**, 24 (1946).

[8] A. W. Chao, *Physics of Collective Beams Instabilities in High Energy Accelerators*, edited by I. John Wiley & Sons (John Wiley and Sons, Inc, New York, 1993).

[9] X. Buffat, L. Barraud, E. Métral, A. Ribes Metidieri, J. Barranco Garcia, P. Goncalves Jorge, T. Pieloni, and C. Tambasco, *Status of the studies on collective effects involving beam-beam interactions at the HL-LHC*, CERN-ACC-NOTE-2018-0036 (CERN, Geneva, Switzerland, 2018).

[10] J. Gareyte, J.-P. Koutchouk, and F. Ruggiero, *Landau damping, dynamic aperture and octupole in LHC*, LHC Project Report 91 (CERN, Geneva, Switzerland, 1997).

[11] D. Amorim, S. Antipov, N. Biancacci, B. Salvant, P. Arpaia, M. Barnes, E. Bonanno, R. Calaga, E. Carideo, H. A. Day, O. Frasciello, F. Giordano, Z. T. Jin, T. R. Kaltenbacher, Z. Li, G. Mazzacano, E. Metral, J. A. Mitchell, N. Mounet, K. N. Sjobaek, L. Vega Cid, V. Vlachodimitropoulos, N. Wang, R. Wanzenberg, C. Zannini, and M. Zobov, *HL-LHC impedance and related effects*, CERN-ACC-NOTE-2018-0087 (CERN, Geneva, 2018).

[12] N. Mounet, D. Amorim, S. Antipov, N. Biancacci, X. Buffat, B. Salvant, and C.Zannini, "Update on the difference between old and new HL-LHC impedance model," Presented at the HL-LHC WP2 meeting, CERN, Geneva `https://indico.cern.ch/event/903324/contributions/3801874/attachments/2023510/3384943/NMounet_20200421_HLLHC_imp_WP2.pdf` (21st Apr. 2020).

[13] `https://impedance.web.cern.ch/`.

[14] X. Buffat, D. Amorim, S. Antipov, L. Carver, N. Biancacci, S. Furuseth, T. Levens, E. Métral, T. P. N. Mounet, B. Salvant, M. Soderen, C. Tambasco, and D. Valuch, "Impact of noise on beam stability," Presented at the 8th HL-LHC Collaboration Meeting, CERN, Geneva https://indico.cern.ch/event/742082/contributions/3084844/attachments/1733747/2804478/2018-10-16_ImpactOfNoiseOnBeamStability-expanded.pdf (11th Oct. 2018).

[15] S. Furuseth and X. Buffat, "Change of the beam distribution due to decoherence in the presence of transverse feedback," in *Proceedings of IPAC2019*, Melbourne, Australia, 19-24 May. 2019 (Jacow, Geneva, Switzerland).

[16] E. Métral and A. Verdier, *Stability diagram for Landau damping with a beam collimated at an arbitrary number of sigmas*, CERN-AB-2004-019-ABP (CERN, Geneva, 2004).

[17] D. Mirarchi, Private communication (9th Sep. 2020).

[18] E. H. Maclean, R. Tomás, F. S. Carlier, M. S. Camillocci, J. W. Dilly, J. Coello de Portugal, E. Fol, K. Fuchsberger, A. Garcia-Tabares Valdivieso, M. Giovannozzi, M. Hofer, L. Malina, T. H. B. Persson, P. K. Skowronski, and A. Wegscheider, "New approach to LHC optics commissioning for the nonlinear era," Phys. Rev. Accel. Beams **22**, 061004 (2019).

[19] R. Jacobsson, "Future wishes and constraints for the experiments at the LHC for the proton-proton program," in *Proceedings of the ICFA Mini-workshop on beam-beam effects in hadron colliders*, Geneva, Switzerland, 18-22 March 2013, edited by W. Herr and G. Papotti (CERN, Geneva, Switzerland, 2014) pp. 167–176.

[20] S. Antipov, "Monitoring status," Presented at the LHC Instability Monitoring Meeting, CERN, Geneva https://indico.cern.ch/event/731326/contributions/3015114/attachments/1654307/2647512/LHC_Instability_Observations.pdf (23th May 2018).

[21] http://cern.ch/mad.

[22] F. Schmidt, E. Forest, and E. McIntosh, *Introduction to the polymorphic tracking code: Fibre bundles, polymorphic Taylor types and "Exact tracking"*, CERN-SL-2002-044-AP (CERN, Geneva, 2002).

[23] "HL-LHC optics repository," https://espace.cern.ch/HiLumi/WP2/task2/SitePages/Home.aspx.

[24] L. R. Carver, X. Buffat, K. Li, E. Métral, and M. Schenk, "Transverse beam instabilities in the presence of linear coupling in the large hadron collider," Phys. Rev. Accel. Beams **21**, 044401 (2018).

[25] N. Karastathis and Y. Papaphilippou, *Beam-beam simulations for optimizing the performance of the High-luminosity Large Hadron Collider Proton Physics*, CERN-ACC-NOTE-2020-0026 (CERN, Geneva, Switzerland, 2020).

[26] R. Tomás, T. H. B. Persson, and E. H. Maclean, "Amplitude dependent closest tune approach," Phys. Rev. Accel. Beams **19**, 071003 (2016).

[27] X. Buffat, E. Maclean, E. Métral, and R. Tomas, "Stability diagrams with lattice non-linearities," Presentation at the Hadron Synchrotron Collective effects section meeting, CERN, Geneva, https://indico.cern.ch/event/677574/contributions/2773931/attachments/1552926/2440695/2017-11-06_stabilityDiagramWithLatticeNL-expanded.pdf (6 Nov. 2017).

[28] T. Persson, "Linear coupling in 2012 and 2016," Presented at the half-day internal review of LHC performance limitations, CERN, Geneva (linked to transverse collective effects) during run II https://indico.cern.ch/event/589625/sessions/215346/attachments/1379197/2095835/coupling_instability_day.pdf (29th Nov. 2016).

[29] L. Ponce, "Tune and orbit feedbacks performance : a user perspective," in *Proceedings of the 2011 Evian workshop on LHC beam operation*, Evian-les-Bains, France, 12-14 December 2011, edited by B. Goddard and S. Dubourg (CERN, Geneva, Switzerland).

[30] T. Lefevre, M. Andersen, C. Boccard, S. Bozyigit, E. Calvo, M. Favier, J. Fullerton, M. Gasior, S. Jackson, L. Jensen, R. Jones, A. Margiolakis, A. Nosych, J. Savioz, R. Steinhagen, M. Wendt, and J. Wenninger, "What you get: Orbit and tune measurement and feedback," in *Proceedings of the 2012 Evian workshop on LHC beam operation*, Evian-les-Bains, France, 17-20 December 2012, edited by B. Goddard and S. Dubourg (CERN, Geneva, Switzerland).

[31] G. Arduini, "(clear?) summary of the observations on instabilities," Presentation at the LHC Machine Committee, CERN, Geneva (15 Aug. 2012).

[32] N. Mounet, X. Buffat, L. Carver, and E. Mértal, "Rescaling the 2015 LHC octupole threshold measurements," Presentation at the Hadron Synchrotron Collective effects section meeting, CERN, Geneva https://indico.cern.ch/event/795854/contributions/3322974/attachments/1797576/2934764/20190218_HSC_rescaling_2015_measurements_NMounet.pdf (18 Feb. 2019).

[33] A. Oeftiger, "Stability around Q'=0," Presentation at the HL-LHC WP2 meeting, CERN, Geneva, https://indico.cern.ch/event/804350/contributions/3394378/attachments/1830532/2997717/oeftiger_damper_instability.pdf (16 Apr. 2019).

[34] X. Buffat, "Impact of the longitudinal distribution on the transverse stability at flat top in the LHC," Presentation at the Hadron Synchrotron Collective effects section meeting, CERN, Geneva https://indico.cern.ch/event/942621/contributions/3960847/attachments/2080506/3494417/2020-06_SineHoledGaussian-expanded.pdf (10 Aug. 2020).

[35] X. Buffat, G. Arduini, D. Amorim, S. Antipov, N. Biancacci, L. Carver, S. Furuseth, G. Iadarola, K. Li, L. Mether, E. Métral, N. Mounet, A. Oeftiger, G. R. A. Romano, B. Salvant, M. Schenk, T. Pieloni, and C. Tambasco, "Transverse instabilities," in *Proceedings of the 2019 Evian workshop on LHC beam operation*, Evian-les-Bains, France, 30 Jan.-1 Feb. 2019, edited by M. Schauman, D. Walsh, and S. Dubourg (CERN, Geneva, Switzerland).

[36] D. Amorim, S. Antipov, N. Biancacci, X. Buffat, E. Carideo, L. Carver, A. Mereghetti, E. Métral, N. Mounet, A. Oeftiger, T. Pieloni, B. .Salvant, and C. Tambasco, "Comparison of LHC impedance model predictions to beam-based measurements," Presentation at the Hadron Synchrotron Collective effects section meeting, CERN, Geneva (4 Mar. 2019).

[37] N. Mounet, "Stability diagrams, damper, mode coupling and all that sort of things," Presentation at the Hadron Synchrotron Collective effects section meeting, CERN, Geneva https://indico.cern.ch/event/794757/contributions/3302064/attachments/1789936/2916065/20190204_HSC_TMCI_tunespread_NMounet.pdf (4 Feb. 2019).

[38] T. Persson, F. Carlier, J. C. de Portugal, A. G.-T. Valdivieso, A. Langner, E. H. Maclean, L. Malina, P. Skowronski, B. Salvant, R. Tomás, and A. C. G. Bonilla, "LHC optics commissioning: A journey towards 1% optics control," Phys. Rev. Accel. Beams **20**, 061002 (2017).

[39] A. Ribes Metidieri and X. Buffat, *Studies of PACMAN effects in the HL-LHC*, CERN-ACC-NOTE-2019-0037 (CERN, Geneva, Switzerland, 2019).

[40] D. Neuffer and S. Peggs, *Beam-beam tune shift and spreads in the SSC - Head on, long range and PACMAN conditions*, SSC-63 (Superconducting Super Collider Laboratory, Dallas, USA, 1986).

[41] X. Buffat, W. Herr, N. Mounet, T. Pieloni, and S. White, "Stability diagrams of colliding beams in the large hadron collider," Phys. Rev. ST Accel. Beams **17**, 111002 (2014).

[42] S. Fartoukh, "On the sign of the LHC octupoles," Presented at the LHC Machine Committee, CERN, Geneva, https://espace.cern.ch/lhc-machine-committee/Presentations/1/lmc_141/lmc_141h.pdf (11th July 2012).

[43] X. Buffat, *Transverse beams stability studies at the Large Hadron Collider*, Ph.D. thesis, EPFL (2015), CERN-THESIS-2014-246.

[44] K. Hirata, H. Moshammer, and F. Ruggiero, "A symplectic beam-beam interaction with energy change," Part.Accel. **40**, 205 (1993).

[45] S. Fartoukh, "Achromatic telescopic squeezing scheme and application to the lhc and its luminosity upgrade," Phys. Rev. ST Accel. Beams **16**, 111002 (2013).

[46] X. Buffat, "Taming the high intensity beam-beam and impedance," Presented at the Aries Workshop on Mitigation Approaches for Storage Rings and Synchrotrons https://indico.gsi.de/event/10458/contributions/45026/attachments/31812/40332/MitigationStragegiesGSI2020-expanded.pdf (24th Jun. 2020).

[47] S. Fartoukh, et al., *Round ATS optics with large tele-index*, CERN-ACC-NOTE-2019 (CERN, Geneva, Switzerland, 2019).

[48] S. Fartoukh, N. Karastathis, L. Ponce, M. Solfaroli Camillocci, and R. Tomas Garcia, *About flat telescopic optics for the future operation of the LHC*, CERN-ACC-2018-0018 (CERN, Geneva, 2018).

[49] C. Tambasco, *Beam Transfer Function measurements and transverse beam stability studies for the Large Hadron Collider and its High Luminosity upgrade*, Ph.D. thesis, EPFL (2017).

[50] D. Gamba, G. Arduini, M. Cerqueira Bastos, J. M. Coello De Portugal Martinez Vazquez, R. De Maria, M. Giovannozzi, M. Martino, and R. Tomas Garcia, *Beam dynamics requirements for HL-LHC electrical circuits*, CERN-ACC-2017-0101 (CERN, Geneva, 2017).

[51] A. Gorzawski, *Luminosity control and beam orbit stability with beta star leveling at LHC and HL-LHC*, Ph.D. thesis, EPFL (2016), CERN-THESIS-2016-193.

[52] E. Métral, G. Arduini, D. Banfi, J. Barranco, H. Bartosik, X. Buffat, O. Bruning, S. Fartoukh, W. Herr, W. Hofle, G. Iadarola, M. Kuhn, K. Li, N. Mounet, T. Pieloni, G. Rumolo, B. Salvachua Ferrando, F. Zimmermann, A. Burov, and S. White, *Summary of the 2-day internal review of LHC performance limitations (linked to transverse collective effects) during run I (CERN, 25-26/09/2013)*, CERN-ACC-NOTE-2014-0006 (CERN, Geneva, 2014).

[53] X. Buffat, G. Arduini, D. Amorim, S. Antipov, L. Barraud, N. Biancacci, F. Giordano, G. Iadarola, G. Mazzacano, E. Métral, B. Salvant, M. Soderen, and D. Valuch, "Our understanding of the instabilities and mitigation tools/strategy," in *Proceedings of the 2017 Evian workshop on LHC beam operation*, Evian-les-Bains, France, 12-14 Dec. 2017, edited by T. Argyropoulos, S. Dubourg, and G. Trad (CERN, Geneva, Switzerland).

[54] S. Fartoukh, D. Amorim, S. Antipov, C. Bracco, R. Bruce, X. Buffat, F. S. Carlier, J. M. Coello De Portugal Martinez Vazquez, N. Fuster Martinez, A. Garcia-Tabares Valdivieso, N. Karastathis, E. H. Maclean, L. Malina, A. Mereghetti, E. Metral, D. Mirarchi, P. S. Papadopoulou, Y. Papaphilippou, T. H. B. Persson, M. Pojer, L. Ponce, A. Poyet, S. Redaelli, B. M. Salvachua Ferrando, P. K. Skowronski, M. Solfaroli Camillocci, G. Sterbini, R. Tomas Garcia, D. Valuch, A. Wegscheider, and J. Wenninger, *Round telescopic optics with large telescopic index*, CERN-ACC-2018-0032 (CERN, Geneva, 2018).

[55] S. Redaelli, S. Antipov, N. Biancacci, A. Bertarelli, R. Bruce, F. Carra, G. Gobbi, A. Lechner, A. Mereghetti, and E. Metral, "Staged implementation of low-impedance collimation in IR7: plans for LS2," (2019).

[56] S. A. Antipov, C. Accettura, D. Amorim, A. Bertarelli, N. Biancacci, R. Bruce, E. Carideo, F. Carra, J. Guardia Valenzuela, A. Mereghetti, E. Métral, S. Redaelli, B. Salvant, and D. Valuch, "Transverse beam stability with low-impedance collimators in the high-luminosity large hadron collider: Status and challenges," Phys. Rev. Accel. Beams **23**, 034403 (2020).

[57] N. Mounet, D. Amorim, S. Antipov, N. Biancacci, X. Buffat, B. Salvant, and C.Zannini, "Update on the HL-LHC impedance model in the new operational scenario,and considerations on crab cavity HOMs," Presented at the HL-LHC WP2 meeting, CERN, Geneva https://indico.cern.ch/event/934794/contributions/3927359/attachments/2080855/3496934/NMounet_20200728_HLLHC_imp_WP2_crab.pdf (28th Jul. 2020).

[58] R. D. Maria, D. Gamba, and F. Plassard, "HL-LHC V1.4," Presented at the HL-LHC Technical Coordination Committee Meeting, CERN, Geneva https://indico.cern.ch/event/758028/contributions/3143207/attachments/1719731/2775919/HL14-TCC3.pdf (20th Sept. 2018).

[59] P. Hagen, M. Giovannozzi, J.-P. Koutchouk, T. Risselada, S. Sanfilippo, E. Todesco, and E. Wildner, *WISE: An Adaptative Simulation of the LHC Optics*, CERN-LHC-Project-Report-971 (CERN, Geneva, 2006).

[60] M. Guthoff and D. Lazic, "CMS requirements for non-colliding bunches in HL-LHC," Presented at the Experimental Data Quality Working Group meeting, CERN, Geneva https://indico.cern.ch/event/672484/contributions/2751113/attachments/1541969/2418575/20171017_EDQ_MG_DL.pdf (17th Oct. 2017).

[61] S. Gibson, S. D. Auria, P. B, and M. Huhtinen, "Non-colliding bunches at HL-LHC," Presented at the Experimental Data Quality Working Group meeting, CERN, Geneva https://indico.cern.ch/event/672484/contributions/2751113/attachments/1541969/2418698/20171017EDQ_ATLAS.pdf (17th Oct. 2017).

[62] F. Schmidt, *SIXTRACK version 1.2: single particle tracking code treating transverse motion with synchrotron oscillations in a symplectic manner; user's reference manual*, CERN-SL-94-56-AP (CERN, Geneva, 1994).

[63] N. Karastathis, R. De Maria, S. Fartoukh, Y. Papaphilippou, and D. Pellegrini, "Refining the HL-LHC operational settings with inputs from dynamic aperture simulations: A progress report," in *Proceedings of IPAC2018*, Vancouver, Canada, 29 Apr. -4 May 2018 (Jacow, Geneva, Switzerland).

[64] S. Furuseth, X. Buffat, and N. Mounet, "Instability latency in the HL-LHC - a first look at crab cavities," Presented at the HL-LHC WP2 meeting, CERN, Geneva https://indico.cern.ch/event/934794/contributions/3927355/attachments/2080801/3494946/Presentation_2020_7_28_L2D2_AFirstLookAtCrabCavities.pdf (28th Jul. 2020).

[65] J. B. Garcia and T. Pieloni, *Global compensation of long-range beam-beam effects with octupole-magnets: dynamic aperture simulations for the HL-LHC case andpossible usage in LHC and FCC*, CERN-ACC-NOTE-2017-036 (CERN, Geneva, Switzerland, 2017).

[66] S. Kostoglou, R. D. Maria, G. Iadarola, S. Kostoglou, Y. Papaphilippou, and G. Sterbini, "Beam-beam DA simulations with new operational scenario," Presentation at the HL-LHC WP2 meeting, CERN, Geneva, https://indico.cern.ch/event/950636/contributions/4021498/attachments/2111177/3551294/HL_LHC_tunescans_newoperationalscenario.pdf (29 sept. 2020).

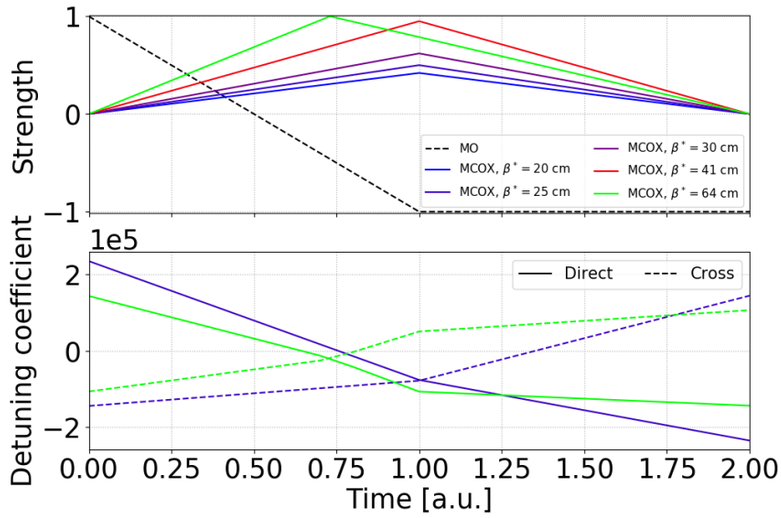

Figure 13: Strengths of the arc octupoles (MO) and of the IR octupole correctors (MCOX), normalised to their respective maximum, during a flip of the arc octupole polarity (upper plot). All octupole correctors are powered with the positive sign, following MAD-X convention. The MCOX strength is adjusted to maximise the negative detuning terms during the process for different β^*. The corresponding direct and cross amplitude detuning with the transverse action were obtained with MADX/PTC normal [21, 22] for the HL-LHC optics V1.3 [23] (lower plot). For readability only the configurations with $\beta^* = 20$ and 64 cm are shown (blue and green curves respectively).

A Polarity flip aided by the MCOX

To increase the robustness of the octupole polarity flip with colliding beams, one may use the octupole correctors in IRs 1 and 5 to maintain Landau damping for the non-colliding bunches. By increasing and decreasing their strengths dynamically during the arc octupole polarity flip as illustrated in Fig. 13, either the direct or the indirect detuning terms remain negative at all times during the process. As a result, Landau damping is never fully suppressed for coherent modes with a negative real tune shift. We note that the contribution of the arc octupoles to the amplitude detuning depends on β^* due to the telescopic optics. Similarly, the contribution of the IR octupole correctors varies strongly with β^* as they are located in the triplet.

Figure 14 shows the evolution of the stability diagram together with the corresponding coherent stability factor. We find that an arc octupole polarity reversal can be performed without transient loss of Landau damping only with a β^* of 30 cm or lower with this scheme.

We note that, due to the presence of a crossing angle, feed down effects to orbit and tunes are expected and require a dedicated correction. The impact on dynamic aperture seems acceptable (Fig. 15).

Since the MCOX act on both beams and generate a detuning with opposite signs, the procedure would need to be performed on one beam after the other. The local correctors in the triplet used to maintain Landau damping during a flip of the polarity of the arc, as discussed in Sec 3.5, introduce a strong local non-linearity which may affect the beam lifetime during the transient. The dynamic aperture simulations in the corresponding configuration show that it remains acceptable.

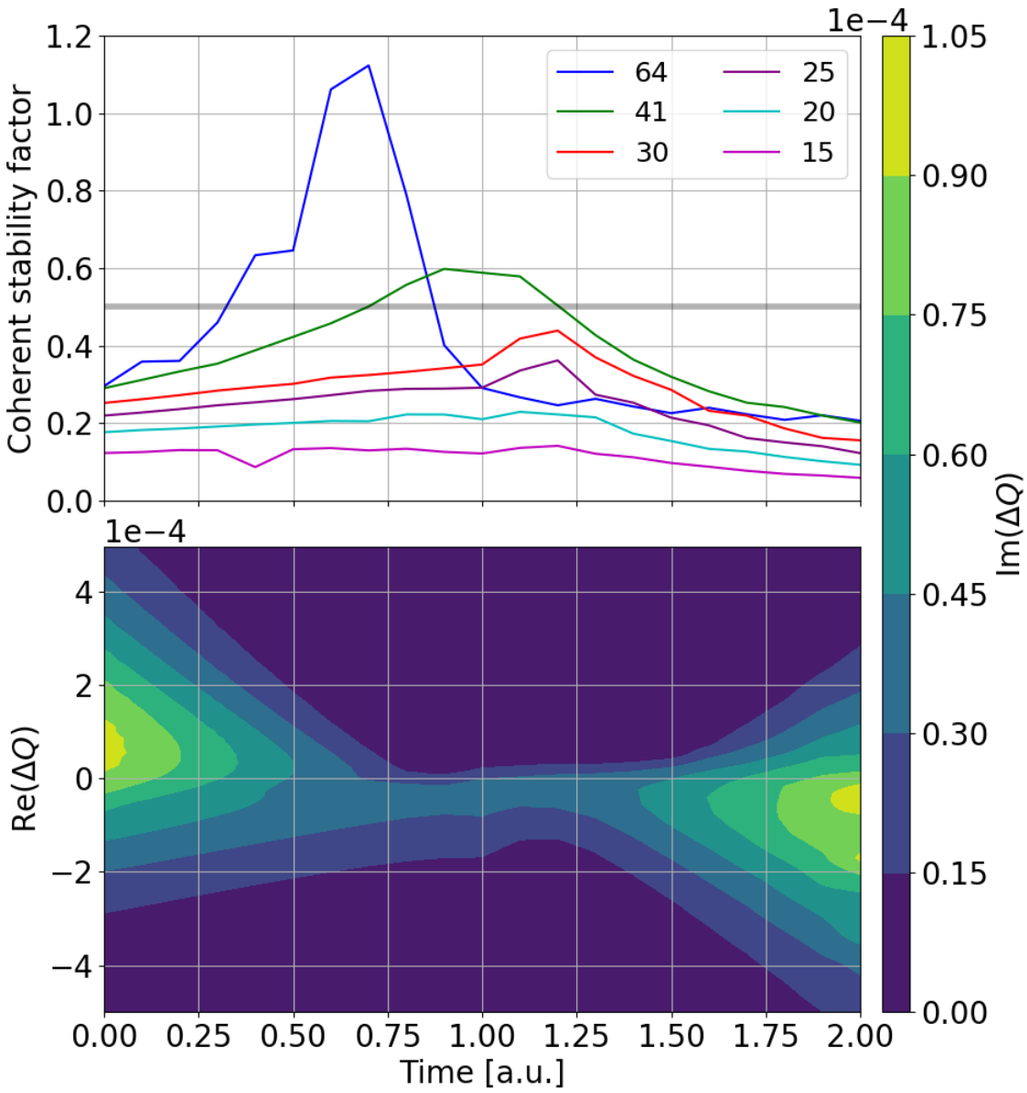

Figure 14: Coherent stability factor obtained for the arc octupole polarity flip described in Fig. 13 for different β^* (in cm, upper plot). The baseline HL-LHC impedance model was considered (Sec. 3.1). A grey horizontal line marks the maximum allowed to maintain Landau damping, including the empirical factor 2. The corresponding evolution of the stability diagram computed with PySSD for $\beta^* = 30$ cm is shown on the lower plot.

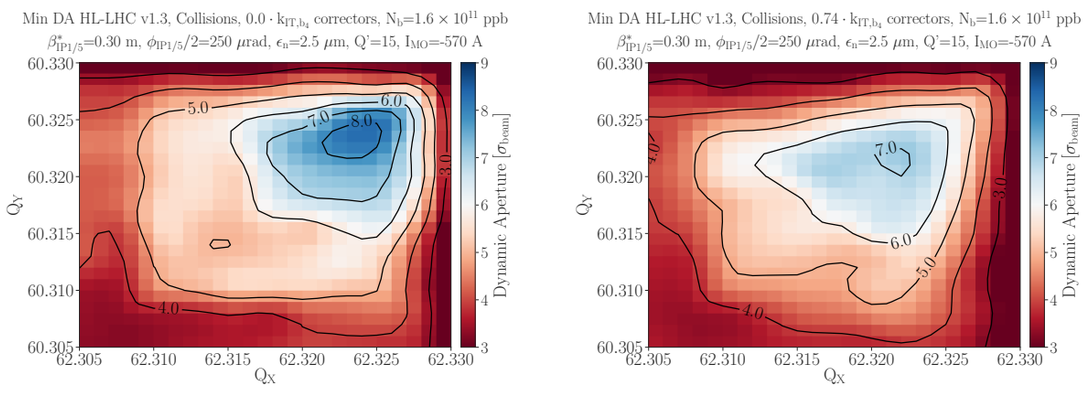

(a) $k_{MCOX} = 0$

(b) $k_{MCOX} = 0.74 k_{MCOX,max}$

Figure 15: Dynamic aperture simulations based on Sixtrack [62] using the HL-LHC optics V1.3 [23] with beam-beam interactions in all interactions points and without magnetic errors [63]. The machine and beam parameters are those of the ultimate HL-LHC scenario [2] at β^* of 30 cm, including the intensity decay. The octupole correctors of the inner triplet are either off (left plot) or powered with the same polarity (MAD-X convention) with the strength corresponding to the optimum described in Fig 13.

B Detuning coefficients

Table 4: Detuning generated by the Landau octupoles uniformly powered with 570A $[10^3\,\mathrm{m}^{-1}]$ for a non-telescopic optics. (HL-LHC optics V1.3 [23], B1)

$\frac{\partial Q_x}{\partial \varepsilon_x}$	$\frac{\partial Q_y}{\partial \varepsilon_x}$	$\frac{\partial Q_y}{\partial \varepsilon_y}$
-140	+100	-136

Table 5: Detuning values of the bare machine which is dominated by second-order contribution from arc sextupoles. (HL-LHC optics V1.3 [23], B1)

β^*	$\frac{\partial Q_x}{\partial \varepsilon_x}$	$\frac{\partial Q_y}{\partial \varepsilon_x}$	$\frac{\partial Q_y}{\partial \varepsilon_y}$
$[m]$	$[10^3\,\mathrm{m}^{-1}]$		
3.00	-0.2	-2.2	-0.9
0.64	0.6	-4.7	1.3
0.41	2.1	-8.1	2.4
0.15	24.0	-41.3	19.8

Table 6: Detuning values when including normal/skew sextupoles and normal/skew octupoles with their ideal corrections. The detuning in this case is dominated by the second order contribution of the arc sextupoles and the residual detuning from b4 correction in IRs 1 and 5. (HL-LHC optics V1.3 [23], B1)

β^*	$\frac{\partial Q_x}{\partial \varepsilon_x}$	$\frac{\partial Q_y}{\partial \varepsilon_x}$	$\frac{\partial Q_y}{\partial \varepsilon_y}$
$[m]$	$[10^3\,\mathrm{m}^{-1}]$		
3.00	5.0	-5.0	-1.4
0.64	7.0	-8.0	2.0
0.41	12.0	-14.0	-3.0
0.15	80.0	-80.0	-20.0

Table 7: Maximum shifts to detuning coefficients when including normal/skew sextupoles and normal/skew octupoles with their ideal corrections. The shifts are dominated by the residual detuning from b4 correction in IRs 1 and 5. (HL-LHC optics V1.3 [23], B1)

β^*	$\Delta\frac{\partial Q_x}{\partial \varepsilon_x}$	$\Delta\frac{\partial Q_y}{\partial \varepsilon_x}$	$\Delta\frac{\partial Q_y}{\partial \varepsilon_y}$
$[m]$	$[10^3\,\mathrm{m}^{-1}]$		
3.00	5	3	-0.5
0.64	6.5	+4	1
0.41	10	+10	-5
0.15	56	+76	-40

Table 8: Current in the Landau octupoles expressed in amperes that yields an identical shift of cross-term detuning coefficient for each source added to the model. The values obtained with the worst seed, i.e. largest positive and negative shifts to amplitude detuning, are shown. The label corr and FD indicated the corrected multipoles and feed-down contributions included in the estimate. (HL-LHC optics V1.3 [23], B1)

β^*	detuning shift from:			
$[m]$	corr(b4)	FD(ab56)	FD(ab56)+corr(ab56)	higher orders
0.64	+29	+60	+22	+15
	-19	-38	-12	-6
0.41	+59	+136	+42	+21
	-30	-95	-23	-11
0.15	+438	+961	+106	+90
	-230	-766	-59	-88

Table 9: Current in the Landau octupoles expressed in amperes that yields an identical shift of the direct detuning coefficient for each source added to the model. The values obtained with the worst seed, i.e. largest positive and negative shifts to amplitude detuning, are shown. The label corr and FD indicated the corrected multipoles and feed-down contributions included in the estimate. (HL-LHC optics V1.3 [23], B1)

β^*	detuning shift from:			
$[m]$	corr(b4)	FD(ab56)	FD(ab56)+corr(ab56)	highorder
0.64	+9	+44	+10	+8
	-26	-30	-5	-4
0.41	+20	+104	+17	+12
	-40	-72	-7	-8
0.15	+166	+740	+268	+97
	-228	-590	-161	-66